Title: BEHAV3D Tumor Profiler to map heterogeneous cancer cell behavior in the tumor microenvironment

Emilio Rios-Jimenez*[1], Anoek Zomer*[2,3], Raphael Collot[2,3], Mario Barrera Román[2,3], Sandra F. Archidona[1], Hendrikus C.R. Ariese[2,3], Ravian L. van Ineveld[2,3], Michiel Kleinnijenhuis[2,3], Nils Bessler[2,3], Hannah Johnson[2,3], Caleb A. Dawson[4,5,6], Anne Rios[2,3] #, Maria Alieva[1] #.

* Equal contribution

Shared last authorship

Affiliations:

[1]Institute for Biomedical Research Sols-Morreale (IIBM), Spanish National Research Council-Universidad Autónoma de Madrid, Madrid, Spain.

[2]Princess Máxima Center for Pediatric Oncology, Utrecht, the Netherlands.

[3]Oncode Institute, Utrecht, the Netherlands.

[4]ACRF Cancer Biology and Stem Cells Division, The Walter and Eliza Hall Institute of Medical Research, Parkville, VIC 3052, Australia.

[5]Immunology Division, The Walter and Eliza Hall Institute of Medical Research, Parkville, VIC 3052, Australia.

[6]Department of Medical Biology, The University of Melbourne, Parkville, VIC 3010, Australia

Abstract

Intravital microscopy (IVM) enables live imaging of animals at single-cell level, offering essential insights into cancer progression. This technique allows for the observation of single-cell behaviors within their natural 3D tissue environments, shedding light on how genetic and microenvironmental changes influence the complex dynamics of tumors. IVM generates highly complex datasets that often exceed the analytical capacity of traditional uni-parametric approaches, which can neglect single-cell heterogeneous in vivo behavior and limit insights into microenvironmental influences on cellular behavior. To overcome these limitations, we present BEHAV3D Tumor Profiler (BEHAV3D-TP), a computational framework that enables unbiased single-cell classification based on a range of morphological, environmental and dynamic single cell features. BEHAV3D-TP integrates with widely used 2D and 3D image processing pipelines, enabling researchers without advanced computational expertise to profile cancer and healthy cell dynamics in IVM data. Here, we apply BEHAV3D-TP to study diffuse midline glioma (DMG), a highly aggressive pediatric brain tumor characterized by invasive progression. By extending BEHAV3D-TP to incorporate tumor microenvironment (TME) data from IVM or fixed correlative imaging, we demonstrate that distinct migratory behaviors of DMG cells are associated with specific TME components, including tumor-associated macrophages and vasculature. BEHAV3D-TP enhances the accessibility of computational tools for analyzing the complex behaviors of cancer cells and their interactions with the TME in IVM data.

INTRODUCTION

Cancer is a complex disease driven by a sequence of genetic and microenvironmental changes. As a result, tumors comprise many different cell populations that are in constant evolution[1] . This tumor heterogeneity has important biological and clinical implications as it differentially promotes key characteristics of individual cancer cells, including proliferation, invasion, and drug resistance [2]. Yet, we are far from fully understanding all the dynamic and bi-directional interactions in heterogeneous tumors, and how these interactions influence cancer cell behavior at the single-cell level. Emerging single-cell technologies and analysis tools provide a new opportunity to profile individual cells within tumors. For example, recent spatial transcriptomic and proteomic profiling provides evidence for the existence of multiple distinct microenvironmental niches within one tumor [3]. However, these techniques can only provide static information and make use of thin tissue sections that are only one cell layer thick. To investigate the real-time behavior of individual cells intravital microscopy (IVM) has been developed to study tumor cell behavior evolution over time but also in their three-dimensional native tissue environment.

IVM is a technique used to capture both spatial and temporal information at a single-cell level in living animals. Over the past years, it has provided many new insights into the dynamics of tumor heterogeneity and the development of therapy resistance [4–15] . For example, intravital imaging of mouse breast cancer models revealed that only a small portion of tumor cells is motile [15], and that fast- and slow-migrating cells are present in distinct regions of the tumor [7,16]. Moreover, additional heterogeneity exists among migrating tumor cells that can, for instance, move randomly or directionally relative to other tumor cells and/or surrounding healthy tissue [7]. However, traditional IVM analyses have considered cancer cells or the tumor microenvironment (TME) as a homogeneous population, thereby ignoring heterogeneity at the single-cell level and the influence of the local microenvironment, where interactions between neighboring cells may affect cellular behavior. To address these complexities, recent studies have used unbiased approaches using morpho-kinetic parameters derived from live *in vitro*[17] or *in vivo* imaging to classify cells and explore the single-cell behavioral landscape as an additional omic layer [18–20]. In line with this concept of characterizing cellular dynamic properties for cell classification, we have previously developed an analytical platform termed BEHAV3D [19,21] allowing to perform behavioral phenotyping of engineered T cells targeting cancer. While BEHAV3D was initially developed to analyze T cell migratory behavior under controlled in vitro conditions, we sought to expand its application to investigate tumor cell behaviors in IVM

data, where the complexity of the TME presents distinct analytical challenges. This manuscript builds on our foundational work but represents a significant advancement by adapting the pipeline specifically for IVM datasets.

While significant efforts have been made to develop open-source segmentation and tracking tools for live imaging data, including IVM[22–27] fewer tools exist for the unbiased analysis of tumor dynamics. One major barrier is that implementing such analytical methods often requires substantial computational expertise, limiting accessibility for many biomedical researchers conducting IVM experiments. To bridge this gap, we present BEHAV3D Tumor Profiler (BEHAV3D-TP) by providing a robust, user-friendly tool that allows researchers to extract meaningful insights from dynamic cellular behaviors without requiring advanced programming skills. BEHAV3D-TP expands the capabilities of BEHAV3D by incorporating key features designed for *in vivo* tumor cell dynamics (Fig. 1). The pipeline includes extensions that integrate tumor cell behavior with spatial features within the native TME, using either in situ (IVM) or fixed correlative imaging to reveal how distinct spatial niches influence tumor dynamics.

To further facilitate unbiased analysis of tumor dynamics, we developed BEHAV3D-TP as a flexible tool that supports both commercial and open-source data formats, ensuring broad compatibility across different research workflows. The pipeline supports 2D and 3D data formats generated by Imaris and by Fiji plugins such as TrackMate, MTrackJ, and ManualTracking, enabling processing of datasets from the most widely used segmentation and tracking solutions. We demonstrate the versatility and broad applicability of BEHAV3D-TP by applying it to a range of published tumor and healthy tissue IVM datasets.

Next, we focused on Diffuse Midline Glioma (DMG), a highly aggressive pediatric brain tumor characterized by invasive growth and its capacity to spread to other regions of the brain and the spinal cord [28]. Our approach allowed us to observe associations between DMG cell migration behavior and specific microenvironmental factors, including tumor-associated macrophages and vasculature, by visualizing TME components either during or after IVM. In our study, we specifically focused on cancer cell migration as a specific feature of DMG, but our methodology could easily be extended to other cancer cell behaviors such as intravasation or metastatic colonization. Overall, BEHAV3D-TP provides an accessible computational approach for a better understanding of tumor-TME crosstalk and the functional implications of this communication in heterogeneous tumors.

RESULTS

BEHAV3D Tumor Profiler: an accessible tool for mapping heterogeneity in tumor dynamics

To comprehensively map and analyze the dynamic heterogeneity of tumor cells within their TME we developed BEHAV3D-TP [https://github.com/imAIgene-Dream3D/BEHAV3D_Tumor_Profiler]. To enhance accessibility and encourage widespread adoption among researchers studying single tumor cell dynamics in live imaging and inspired by previous work on democratizing advanced image analysis[26,29,30], we designed BEHAV3D-TP as a modular Jupyter Notebook featuring an intuitive graphical user interface (GUI) (Figure 1 and Supplementary Video 1). The platform runs directly in a web browser and requires only a Google account for access. BEHAV3D-TP implementation within the Google Colaboratory (Colab) framework not only ensures efficient cloud-based computation with free and scalable resources but also enhances tool accessibility by eliminating the need for local software installation, a common barrier for inexperienced users. Regardless of programming proficiency, users can navigate the computational pipeline to extract comprehensive insights into tumor dynamics (Figure 1). After time-lapse image file processing and preparation using various frameworks (Figure 1a), the central component of BEHAV3D-TP — called the *heterogeneity module* (Figure 1b) — enables researchers to uncover diverse patterns of tumor morphodynamic behavior. Additionally, we provide two extension modules—the *large-scale phenotyping module* (Figure 1c) and the *small-scale phenotyping module* (Figure 1d)— which integrate tumor cell behavior identified with the *heterogeneity module* with TME features based on different data types. The *large-scale phenotyping* module uses post-IVM fixed imaging data for tissue phenotyping, identifying extensive regions with specific TME characteristics, and assessing the distribution of distinct tumor cell behavioral patterns within these regions. The *small-scale phenotyping* module uses *in situ*-labelled TME structures from IVM data, facilitating the correlation of these TME features within the microenvironment of individual tumor cell neighborhoods. Both modules, in conjunction with the *heterogeneity* module, help to identify how different aspects of the TME influence distinct behavioral patterns of tumor cells.

To evaluate the capability of the BEHAV3D-TP *heterogeneity module* in identifying diverse morphodynamic cell patterns, we applied it to IVM datasets from various tumor and healthy models. The datasets, processed with different segmentation and tracking tools, were analyzed

143 for multivariate similarities in morphological and dynamic features (summarized in Table 1)
144 using the dynamic time warping algorithm[21].

145 As an initial benchmark, we analyzed a previously published IVM dataset of two migratory and
146 metastatic breast cancer cell lines (4T1 and MDA-MB231), tracked in 2D using the MTrackJ
147 Fiji plugin (Supplementary Figure 1a) [15]. BEHAV3D-TP provided a more granular
148 characterization of these behaviors, uncovering additional migratory patterns not reported in
149 the original study (Supplementary Figure 1b-c). Specifically, we identified behaviors such as
150 *Fast*, *Intermediate*, *Very slow* and *Static* that had a different distribution among both tumor cell
151 lines (Supplementary Figure 1d-e).

152 To further assess the versatility of BEHAV3D-TP, we applied it to 2D IVM data of terminal
153 end buds (TEB) from healthy mammary gland tissue[31]. This dataset features confetti-labeled
154 epithelial cell types and was analyzed using maximum intensity projections of multiple z planes
155 showing cell morphology changes. As described in the original publication[31] cell segmentation
156 was performed with Cellpose 2.0[32] within the MaSCOT-AI workflow, followed by tracking
157 using the TrackMate plugin in Fiji. This workflow not only confirmed the compatibility of
158 BEHAV3D-TP with advanced segmentation frameworks but also its usage to unravel distinct
159 morphodynamic patterns in non-tumor epithelial cells (Supplementary Figure 2b,c). Consistent
160 with previous findings that HR+ TEB (Pr-cre/Confetti) exhibit greater migratory capacity than
161 HR- TEB (Elf5-rtTA/TetO-Cre/Confetti), our analysis suggests that this difference is primarily
162 driven by a distinct morphodynamic behavior (Supplementary Figure 2 c,d). Specifically, HR+
163 TEB more frequently exhibited characteristics of Cluster 2, defined by a rounder shape and
164 increased motility. Despite the small sample size requiring further validation, these results
165 demonstrate BEHAV3D-TP's ability to uncover complex, multiparametric cellular behaviors
166 that are often missed in analyses focused on single-value comparisons across conditions.

167 We next tested BEHAV3D-TP with a 3D image processing pipeline applied to IVM data from
168 adult glioma (GBM) [7]. In this case, cells were segmented using µSAM[33], a deep-learning
169 foundation model adapted for microscopy data (Segment Anything for Microscopy), and
170 subsequently tracked with TrackMate[27] Fiji plugin (Supplementary Figure 3a). BEHAV3D-TP
171 identified distinct GBM morphodynamic patterns, each characterized by unique combinations
172 of morphological and dynamic features and associated with specific spatial distributions
173 (Supplementary Figure 3b-d). Cluster 1, consisting of large and slow-moving cells, was more
174 isolated and located farther from neighboring cells compared to Cluster 6 (small, fast, persistent

175 cells) and Cluster 4 (very small, static cells). These findings suggest that the compact spatial
176 arrangement of small cells within the tumor may contribute to their reduced size.

177 Collectively, these findings underscore the versatility and broad applicability of BEHAV3D-
178 TP across diverse biological systems, dimensionalities (2D and 3D), imaging modalities, and
179 data processing pipelines, supporting its utility as a robust tool for the in-depth analysis of
180 cellular behavioral patterns in IVM data.

181 **Identification of highly heterogeneous *in vivo* cell behavior displayed by DMGs**

182 We then applied our platform to get insights into the behavioral heterogeneity among pediatric
183 DMG tumors, characterized by a highly invasive nature. We implanted mice with patient
184 derived DMG cells expressing H2BmNeonGreen marker and performed IVM for up to 5.4
185 hours upon tumor development (Figure supplement 4a). We tracked intravitally imaged DMG
186 cells from different mice using Imaris, a commercial software a widely adapted by the IVM
187 community[34–40] for its intuitive 3D visualization and analysis capabilities. In each imaged
188 position, we evaluated not only the dynamic characteristics of individual DMG cells but also
189 their spatial relationship to the tumor edge, which was delineated using Imaris Surface module
190 (Figure 2a, see Methods). Next, to untangle the complexity of tumor cell dynamics in an
191 unbiased manner, we used the BEHAV3D-TP *heterogeneity module,* implementing
192 multiparametric single-cell time-series classification to identify distinct single-cell behavioral
193 patterns (Figure 2 a, b). For this, we used kinetic parameters, including displacement, speed,
194 persistence, and movement direction relative to the tumor edge (Table 1), followed by
195 dimensionality reduction to classify cells. The BEHAV3D-TP *heterogeneity module* identified
196 7 DMG behavioral clusters: *retreating*, *slow retreating*, *erratic*, *static*, *slow*, *slow invading,* and
197 *invading* (Figure 2b, c, d, Supplementary video 2). To accurately describe each of the clusters,
198 we analyzed their most predominant features (Figure 2d) and back-projected the cluster
199 information into the original time-lapse to visually inspect cell behavior in relation to the tumor
200 (Figure 2a, c, Figure supplement 4b, Supplementary video 2). Of particular interest were cells
201 from the *invading* and *retreating* clusters, characterized by fast movement away from and
202 towards the tumor edge, respectively (Figure 2c-f, and Figure supplement 4c). In fact, in this
203 particular DMG model, approximately 10% of the cancer cells were displaying *invasive*
204 behavior (Figure supplement 4d), in line with the intrinsic infiltrative nature of DMG[41] .
205 Interestingly, about another 10% of DMG cells were moving back to the tumor edge (*retreating*,
206 *slow retreating* clusters) (Figure supplement 4d), behavior that has been previously observed
207 for glioblastoma and suggested to be regulated by differential chemotactic signaling by the

208 tumor edge and the surrounding brain parenchyma[7]. We also observed *erratic* cells that display
209 fast non-directed migration behavior, and *static* cells that are non-migratory (Figure 2c-f).
210 Crucially, the distinct behavioral patterns were detected in all intravitally imaged mice (Figure
211 supplement 4d), ruling out any sample bias that might lead to clusters consisting solely of cells
212 from a single tumor or mouse. This underscores the effectiveness of the BEHAV3D-TP in
213 revealing representative heterogeneous tumor behavioral patterns.

214 Mapping *in vivo* tumor cell migratory properties to distinct TME regions identified 215 through *ex vivo* large-scale 3D imaging

216 To investigate whether the TME influences behavioral heterogeneity among cancer cells, we
217 developed two complementary approaches to correlate the identified behavioral clusters (Figure
218 2) to the composition of the TME (Figures 1c, 3a and 4a).

219 The first approach consists of performing large-scale TME phenotyping and identifying regions
220 with a specific cellular composition and architecture within the TME of intravitally imaged
221 tumors that were subsequently fixed. This is accomplished by using multispectral large-scale
222 single-cell resolution 3D (mLSR-3D) imaging data[42,43] and a spatial analysis framework called
223 CytoMAP[44] (Figure 3a). We selected microenvironmental components of interest, such as
224 perivascular niches and glial cells, as they have been previously reported to play an important
225 role in the invasive behavior of glioblastoma cells[7,45–49]. Specifically, intravitally imaged brains
226 were collected immediately after the IVM imaging sessions and were fixed and stained for
227 blood vessels (CD31), oligodendrocytes (Olig2), and tumor-associated microglia/macrophages
228 (TAMM) (Iba1) (Figure 3b). Subsequent CytoMAP[44] spatial phenotyping analysis identified
229 three different environmental niches: *Void* regions (less vascularized and with low glial
230 infiltration), *TAMM/oligo* regions (enriched in oligodendrocytes, TAMM, and tumor cells), and
231 *TAMM/vascularized* regions (highly vascularized regions enriched in TAMM) (Figure 3b, and
232 Figure supplement 5a-c). To investigate the heterogeneity of tumor cell behavior in relation to
233 the identified microenvironmental niches, BEHAV3D-TP *large-scale phenotyping module*
234 mapped the different niches (*Void*, *TAMM/Oligo*, and *TAMM/vascularized*) identified by
235 CytoMAP onto 3D intravital imaging data (Figures 1c, 3c). In the TME-defined IVM-imaged
236 positions we compared the frequencies of the different behavioral clusters that we identified
237 with the BEHAV3D-TP *heterogeneity* module (Figure 3d). Interestingly, *invading* cells were
238 more abundant in *TAMM/vascularized* regions compared to *Void* regions that contain a higher
239 proportion of *static* cells, and *TAMM/Oligo* microenvironments contain more *slow retreating*
240 cells compared to the other regions (Figure 3d, Figure supplement 5d). Finally, we compared

241 the results obtained with BEHAV3D-TP to a more classical IVM analysis approach that relies
242 on assessing single dynamic parameters. Interestingly, single parameters showed a restricted
243 ability to identify differences in cellular behavior among various environments (Figure
244 supplement 5e-g), underscoring the importance of multiparametric behavioral mapping in
245 revealing more nuanced cellular behavior that cannot be captured solely by individual dynamic
246 parameters.

247 **Linkage of *in vivo* tumor cell behavior to the composition of the microenvironment at a**
248 **single-cell level**

249 With the goal of further refining TME phenotyping to better understand tumor cell behavior
250 determinants, we implemented an alternative approach using the BEHAV3D-TP *small-scale*
251 *phenotyping module* (Figure 1d, 4a). This module utilizes the detection of TME components
252 during IVM to offer insights into their abundance and spatial relationship with DMG cells at a
253 single-cell level. It complements the *heterogeneity module*, which captures tumor cell
254 behavioral profiles, and offers two options of integration: (1) *upstream integration*, where
255 TME-derived spatial features—such as proximity or interactions with specific components—
256 are used as input variables for clustering tumor cells; and (2) *downstream integration*, where
257 previously defined behavioral clusters are correlated with TME spatial features in a subsequent
258 analytical step (Figures 1d, 4a). When using the upstream integration approach, it is essential
259 to include only biologically meaningful features, as the presence of irrelevant or redundant
260 variables can introduce noise and compromise the interpretability of the resulting clusters.

261 For *in vivo* TME labeling, we injected mice with an anti-CD31-AF647 antibody to label blood
262 vessels, and with either SR101, a fluorescent marker known to label oligodendrocytes and
263 astrocytes [50–53], or CD20r, a novel molecule described to label microglial cells [54] (Figure
264 supplement 6a, b). This allowed us to measure spatial TME characteristics of each single DMG
265 cell, such as minimal distance to a certain TME component, the number of these cell types in a
266 certain radius, or the cell density for this particular cell (Figure 1d). We applied option 2 of the
267 BEHAV3D-TP *small-scale phenotyping module* to explore the local TME context of distinct
268 behavioral DMG clusters, revealing substantial microenvironmental heterogeneity across
269 clusters (Figure 4b). Compared to *static* cells, *invading* cells tended to be more sparsely
270 distributed relative to neighboring DMG cells (Figure 4b, Figure Supplement 6c), consistent
271 with their invasive behavior into the brain parenchyma. In agreement with our large-scale TME
272 phenotyping results (Figure 3), *invading* DMG cells were found to reside in regions enriched
273 with TAMMs (Figure 4b). Specifically, a higher proportion of *invading* cells were in close

proximity to TAMMs compared to *static*, *retreating*, and *slow-retreating* clusters (Figure 4c). They frequently migrated directionally toward TAMMs (Figure 4d, Supplementary Video 3), suggesting that migration of this behavioral cluster is at least partially mediated by chemotaxis. Furthermore, all fast-migrating behavioral clusters (*invading*, *erratic,* and *retreating*) were found to be generally closer to blood vessels (Figure 4b and e), suggesting that perivascular invasion is a more efficient movement route for these cells (Figure 4f), a mode of migration that has been previously observed for adult glioblastoma cells as well [7,45,47–49]. Lastly, particularly *slow-retreating* DMG cells were found in regions enriched for $SR101^{+}$ cells (Figure 4b and Figure supplement 6d), perhaps reflecting oligodendrocyte-like (OC-like) tumor DMG cells that have been found near oligodendrocytes [55]. Altogether, these data demonstrate the power of our BEHAV3D-TP pipeline in correlating single-cell tumor cell behavior to its local environment, with an important opportunity to identify novel environmental regulators of invasion.

DISCUSSION

Here, we provide a new user-friendly platform tailored for IVM single tumor cell dynamics analysis, termed BEHAV3D-TP, aiming to better understand the mechanisms underlying tumor heterogeneity. In contrast to traditional pipelines that rely on the analysis of single parameters such as cell speed or displacement[56–58] or that use an artificial threshold to assign a specific behavior to cells[10], BEHAV3D-TP is an unbiased approach based on the integration of multiple parameters measured by IVM. Using the *heterogeneity module* of our BEHAV3D-TP pipeline, we uncovered behavioral phenotypes that have not been described before and that could not have been identified using single parameter analysis. For example, our analysis revealed *invading* and *retreating* clusters, composed of cells with a similar cell speed but with an opposite migration direction, an important biological and clinical difference. Likely, bidirectional migration is mediated by different chemotactic cues and by the composition of the local TME[59]. It is of vital importance for DMG and other cancer patients to better understand the biology underlying the different behavioral phenotypes, especially concerning *invading* cells that are difficult to therapeutically target [60].

Previous studies suggest a major role for the microenvironment in promoting tumor cell spread into the healthy brain [61–63]. Indeed, using the complementary *large-* and *small-scale TME phenotyping modules* of BEHAV3D-TP, we identified substantial differences in the TME composition of the different behavioral DMG clusters. Our results also show that the small-scale TME analysis has a higher predictive value compared to the large-scale TME analysis,

suggesting that a cell's direct microenvironment is a more important regulator of its behavior compared to its macroenvironment. Future experiments directed towards identifying more TME components, for example using multispectral LSR-3D imaging[42], could therefore further refine the *large-scale phenotyping module* by detecting subregion heterogeneity.

IVM enables simultaneous labeling of various TME components and allows real-time investigation of their association with tumor cell behavior. Indeed, we found that TAMMs and blood vessels were associated with specific behavioral phenotypes, showing the power of BEHAV3D-TP *small-scale phenotyping module* in identifying novel regulators of cellular behavior. This is exemplified by our finding that *slow-retreating* DMG cells were found in environments enriched for $SR101^{+}$ cells, an observation that has not been made before. To take further advantage of BEHAV3D-TP, future work should be directed toward identifying more TME components, including cells of the adaptive immune system. For example, it would be interesting to use our pipeline on recently developed immunocompetent mouse models of DMG[64,65], or in mice with a humanized immune system[66]. While our findings suggest that microenvironmental factors may influence tumor cell migration, further studies will be necessary to establish causal relationships. Additional experimental validation, such as macrophage ablation experiments, could help clarify the specific contributions of these factors.

While our current study does not provide direct functional validation of the distinct motility clusters identified, existing literature strongly supports the notion that cell dynamics can serve as a proxy for functional states and phenotypic heterogeneity. Prior work, including studies by our group[19,67] as well as Crainiciuc et al.[36] and Freckmann et al.[20], has demonstrated that variations in cell motility patterns can reflect underlying functional characteristics. Specifically, cell morpho-dynamic features have been shown to correlate with differences in cell type identity, T-cell engagement, metastatic potential, and drug resistance states. This growing body of evidence suggests that tumor cell behavior, as captured by BEHAV3D-TP, may serve as a predictive tool for deciphering functional tumor heterogeneity. Future studies integrating transcriptomic or proteomic profiling of motility-defined subpopulations could further elucidate the biological significance of these behavioral phenotypes.

In addition to motility-based classification, features such as tumor cell morphology, proliferation state, and interactions with the TME can further refine tumor phenotyping. BEHAV3D-TP allows for the selection of diverse feature types, supporting datasets that include both dynamic, morphological, spatial and environmental parameters. However, we recognize that expanding the feature set may introduce biologically irrelevant noise, particularly in 3D

microscopy data where limited z-axis resolution can lead to morphological artifacts. This highlights the potential need in the future to include unbiased feature selection strategies, such as bootstrapping methods[68], to ensure the identification of meaningful and biologically relevant parameters. Careful consideration of these aspects is key to maximizing the interpretability and predictive value of analyses performed with BEHAV3D-TP.

To enhance the accessibility of BEHAV3D-TP for researchers keen on studying tumor cell behavioral profiles through live imaging, we have incorporated our software in a Google Colab notebook, allowing researchers with minimal programming skills to employ the tool online without the requirement to install specific software environments nor the need to directly interact with the code. The user can easily install the necessary dependencies, set up the working environment, process datasets and adjust parameters without requiring deep coding skills. Google Colab provides the necessary computational resources to be able to run the pipeline without demanding a powerful local machine. However, there are RAM usage and runtime limitations that could affect the analysis, given a big enough dataset in the free version of Google Colab. Given this and data privacy concerns, the workflow can also be run locally via a Jupyter Notebook, that can be downloaded from the Google Colab notebook. Aligned with the goals of BEHAV3D-TP, other methods utilizing the Google Colab framework are emerging, such as CellTracksColab[29], which is a general tool for tracking data analysis. While CellTracksColab offers valuable insights into tracking data, BEHAV3D-TP is specifically designed for IVM data and includes additional features. These features include directionality metrics crucial for invasion studies, detailed analysis of identified behavioral populations, data back-projection, and correlation of these behaviors with both large-scale and small-scale TME features. This comprehensive approach provides a deeper understanding of the TME drivers behind intratumoral heterogeneity, making BEHAV3D-TP a robust tool for researchers investigating the complex behaviors of tumor cells in their natural environments. BEHAV3D-TP supports a broad range of data formats, including those generated by commercial Imaris and by open-source Fiji plugins such as TrackMate, MTrackJ, and ManualTracking, increasing the tool's applicability to researchers using both commercial and open-source pipelines.

In summary, BEHAV3D-TP allows to get insights into the heterogeneity of tumor cell migration behavior in an accessible way; however, it would be exciting to extend the application to other behaviors, such as cell division or therapy response to study TME-mediated drug resistance.

372 **METHODS**

373 **Animal material**

374 NOD.Cg-PrkdcscidIl2rgtm1Wjl/SzJ (NSG) mice were purchased from Charles River
375 Laboratories (France). Experiments were conducted per Institutional Guidelines under acquired
376 permission from the local Ethical Committee and as per current Dutch laws on Animal
377 Experimentation. Mice were housed under sterile conditions using an individually ventilated
378 cage (IVC) system and were fed with sterile food and water.

379 **Human DMG sphere-forming culture**

380 DMG007 (HSJD-DIPG-007) cells established from primary DMG material were grown in a
381 base medium (TSM) consisting of 48% DMEM/F12 and 48% Neurobasal medium (Thermo
382 Fisher) supplemented with GlutaMAX, 100mM Sodium Pyruvate, MEM non-essential amino
383 acids and 1M Hepes buffer, at 1% each. Primocin (InvivoGen) at 50mg/ml was additionally
384 added to the TSM. Working medium was prepared by adding 20ng/ml of human EGF and
385 human basic FGF, 10ng/ml of PDGF-AA and PDGF-BB (Peprotech) and 2ug/ml of Heparin
386 (StemCell Technologies). DMG cells were cultured at 37 °C in a humidified atmosphere with
387 5% CO_2.

388 **Fluorescent reporter cloning and lentiviral transduction**

389 Fluorescent reporter construct was based on the combination of Histone2B-mNeonGreen, P2A
390 and mScarlet I-CAAX gifted from Dr. Hugo Snippert (UMC Utrecht, The Netherlands), and
391 inserted by In-Fusion HD Cloning Plus (Takarabio) into a lentiviral vector including
392 cPPT/CTS, WPRE, an EF1a promoter and IRES-puromycin-resistance cassette[11]. Subsequently
393 the above-mentioned elements were amplified by PCR and the amplicon was assembled in the
394 final lentiviral backbone using Gibson Assembly (NEB). Sequences were validated using
395 Sanger sequencing. DMG007 cells were transduced using a standard lentiviral transduction
396 protocol and selected using puromycin to achieve a stable cell line.

397 **Cranial imaging window (CIW) surgery and tumor cell injection**

398 CIW surgery and tumor cell injection were performed on the same day as previously described
399 [7,10]. Briefly, mice were sedated with Hypnorm (Fluanison [neuroleptic] + Fentanyl [opioid])
400 (0.4 ml/kg) + Midazolam [benzodiazepine sedative] (2 mg/kg) at a dose of 1:1:2 in sterile water
401 and mounted in a stereotactic frame. The head was secured using a nose clamp and two custom-
402 made 3D printed ear bars, made out of Polylactic Acid (PLA, Geeetech, 700-001-043). The

head was shaved, and the skin was cut circularly. The mouse was placed under a stereo-microscope to ensure precise surgical manipulation. The periosteum was scraped, and a circular groove of 5 mm diameter was drilled over the right parietal bone. The bone flap was lifted under a drop of cortex buffer (125 mM NaCl, 5 mM KCl, 10 mM glucose, 10 mM HEPES buffer, 2 mM $MgSO_4$, and 2 mM $CaCl_2$, pH 7.4), and the dura mater was removed. Gelfoam sponge (Pfizer) was used to stop potential bleedings. Next, 1×10^5 DMG007-H2B-mNeonGreen cells resuspended in 3 µl phosphate-buffered saline (PBS) were injected stereotactically using a 5 µl Hamilton syringe with a 2 pt style in the middle of the craniotomy at a depth of 0.5 mm. The exposed brain was sealed with silicone oil and a 6 mm coverslip was glued on top. Dental acrylic cement (Vertex) was applied on the skull surface, covering the edge of the coverslip, and a custom-made 3D printed ring made of biocompatible Polylactide acid (PLA, Geeetech, 700-001-0433) was glued around the coverslip to provide fixation during intravital imaging and to serve as a reservoir for a water drop required for the objective of the microscope. A single dose of 100 µg/kg of buprenorphine (Temgesic, BD pharmaceutical limited) was administered for post-surgical pain relief. Mice were closely monitored twice per week to assess behavior, reactivity, and appearance.

Intravital imaging

For DMG IVM imaging mice were intravitally imaged as previously described [7,10]. In short, mice were sedated with isoflurane and placed face-down in a stereotactic frame. The Polylactide ring was used to fix the mouse's head to the frame with custom-made Polylactide bars. Time-lapse images of the entire tumor volume were acquired for a maximum of 5.4 hours. The minimal time interval between serial images was set to 20 minutes. For tile scans, images of the complete z-stack of the tumor were acquired, with a step size of 2 µm. In a group of 3 mice, oligodendrocytes and astrocytes were imaged by an intravenous injection of 50 µL SR101 (Thermofisher) at a concentration of 5 mM dissolved in PBS. In a different group of 3 mice, TAMMs were imaged by intravenous injection of 50 µL 100 µM CDr20[54]. Simultaneously with the injection of either SR101 or CDr20, all mice received an intravenous injection of 10 ul CD31-AF647 antibody (ThermoFisher, A14716) to visualize the blood vessels.

Intravital imaging was performed on an upright FVMPE-RS multiphoton microscope (Olympus) equipped with a MaiTai DeepSee and an InSight DeepSee laser (Spectra-Physics), a 25x/1.05 numerical aperture water objective, and two GaAsP and two Multialkali photomultiplier tubes (Olympus). Images were acquired with simultaneous imaging with the MaiTai (960 nm) and Insight (1100 nm) lasers. Green, red, and far-red fluorescence was

436 separated by 570 nm and 650 nm dichroic mirrors, and 610/70 nm and 705/90 nm filters
437 (Semrock) and collected by GaAsP or Multialkali photomultiplier tubes. Scanning was
438 performed in a bidirectional mode with a resonant scanner at 400 Hz and 12 bit, with a zoom of
439 1x, 512 × 512 pixels. For optimal detection of blood vessels (CD31-AF647), a single tile scan
440 was made at the last timepoint with Insight laser tuned at 1250 nm. At the postprocessing step,
441 this image was co-registered to the time-lapse movie.

442 Breast tumor IVM imaging was performed as described before[15] and data was kindly provided
443 by Dr. Nienke Vrisekoop. GBM IVM imaging was performed as described before[7] and data
444 was kindly provided by Prof. Jacco van Rheenen. Breast epithelial IVM imaging and cell
445 tracking with MaSCOT-AI was performed as described before[31] and single cell tracks were
446 downloaded from Zenodo repository (14503476).

447 **Co-registration of IVM imaged blood vessel imaging**

448 CD31-AF647 tile scan featuring optimal visualization of blood vessels during live imaging was
449 co-registered to the last timepoint of the time-lapse movie. Both images (last timepoint of time-
450 lapse tile-scan and blood vessel tile-scan) were visually inspected to determine and annotate the
451 internal landmarks using Imaris (Oxford Instruments), versions 9.5 to 9.6. These landmarks
452 served as a reference for the co-registration software to overlap both images. To perform the
453 co-registration, a modification of *elastix*[69] was used; a python-based open-source software
454 based on Insight Segmentation and Registration Toolkit (ITK) plus SimpleElastix[70] : a
455 collection of different algorithms used on medical image registration. Due to the extensive
456 number of potential parameter combinations, specific parameters were manually chosen. This
457 selection was conducted using the Slicer3D visualization software, version 5.2.2.

458 **Immunohistochemistry**

459 3D immunohistochemistry was performed as described before [43]. After the live imaging session,
460 mouse brains were immersed in 5 ml 4% paraformaldehyde (PFA) pH 7.4 overnight on ice.
461 After fixation, brains were blocked in 5-10 ml Wash Buffer 1 (2 ml Tween-20, 2 ml Triton X-
462 100, 2 ml 10% SDS, and 2 g BSA in 1 l PBS) for 5 hours. For multiplex immunolabeling, a
463 two- or three-round staining protocol was used as previously described[42,43]. Washing and
464 incubation steps were performed in Wash Buffer 2 (1 ml Triton X-100, 2 ml 10% SDS, and 2
465 g BSA in 1 l PBS). A thick (1 mm) slice of the cortex part that was under the cranial imaging
466 window was dissected with a scalpel before proceeding to immunolabeling. The following
467 primary antibodies were used: rabbit anti-Olig2 1:100 (AB9610, Merk), goat anti-Iba1 1:200

468 (NB100-1028SS, NovusBio) and CD31-AF647 1:250 (A14716, ThermoFisher). As secondary
469 antibodies, donkey anti-rabbit AF405 1:250 (ab175651, Abcam) and donkey anti-goat AF633
470 1:250 (A21082, ThermoFisher) were used. After the last washing step, tissues were optically
471 cleared by three stepwise incubations of an increasing concentration of FUnGI[71] clearing agent
472 (25%/50%/75%, diluted in PBS) for 1h at room temperature[42]. The final incubation step with
473 100% FUnGI was performed overnight at 4°C.

474 **mLSR3D imaging**

475 mLSR3D imaging[42,43] of thick slices of fixed mouse cortex was performed using a Zeiss
476 LSM880 system equipped with a 32-channel spectral detector. The signal from all fluorophores
477 present in the samples was collected in a single acquisition and linear unmixing was used to
478 obtain separate channels. Unmixing was carried out by the Online Fingerprinting mode of the
479 microscope. Pre-acquired references of each single fluorophore were used to enable
480 multispectral on-the-fly unmixing. Imaging was performed using a 25x multi-immersion
481 objective 0.8 NA (Zeiss 420852-9871) with a working distance of 570µm. Tile scans were
482 acquired using a voxel size of 0.332x0.332x1.200 µm, a pixel dwell of 2µs, and a 10% tile
483 overlap.

484 **Imaris image processing**

485 DMG IVM datasets were processed using Imaris software (Oxford Instruments, versions 9.5 to
486 10.1) for 3D visualization, shift correction, object rendering, and cell tracking of time-lapse
487 movies.

488 ***Imaris Cell tracking***

489 The *Channel Arithmetics* Xtension was used for channel unmixing of overlapping signals. The
490 Spots ImarisTrack module was used for object detection and semi-automated tracking of tumor
491 cells (autoregressive motion). Tumor cell tracks were manually corrected to ensure accurate
492 tracking. Around 50-100 cells per position were manually corrected and labeled as such for
493 posterior selection of accurate tracks. To determine the direction of tumor cell movement
494 relative to the tumor core, at the image edge closer to the tumor core a "Tumor edge" surface
495 object was manually rendered using the contour tool. The *Distance Transformation* Xtension
496 was used to measure the distance between tumor cells and the "Tumor edge". For tracked tumor
497 cells, time-lapse data containing the coordinates of each cell, the values of cell speed, mean
498 square displacement, displacement delta length, displacement length, and distance to "Tumor

edge" were exported. See https://qbi.uq.edu.au/files/40820/ImarisManual.pdf for statistical details.

Imaris Microenvironmental factors rendering

For rendering the microenvironmental factors detected during IVM or by post-IVM LSR-3D imaging, the Surface and Spots modules of Imaris were used. Surfaces were used for the SR101, CDr20, Olig2, DAPI, and Iba1 stainings, and Spots were used for CD31+ protruding or elongated structures, as previously described [44]. For rendered structures, positional data containing the coordinates of objects were exported for large-scale spatial phenotyping with Cytomap.

Fiji image processing

µSAM cell segmentation

Segmentation was performed using the µSAM plugin for Napari[33] , where *vit-b* model was selected to compute embeddings for each timeframe. Automatic segmentation was applied, and parameters were adjusted for optimal results. Manual corrections were made to remove unwanted surfaces or add missing cells. Once segmentation was complete, frames were combined into a single stack in ImageJ and tracked with Trackmate.

Fiji tracking

Breast tumor IVM data was manually tracked with Fiji MtrackJ plugin as previously described[10,15] .

Adult glioma cells, segmented with µSAM, were consequently tracked with Fiji TrackMate plugin. The labeled image stack, segmented using µSAM, was imported into ImageJ for cell tracking with the Fiji TrackMate plugin. The "Label Image Detector" was employed to identify individual cells, and the LAP Tracker was used to link cells across timeframes. Tracking parameters were optimized to account for missing frames and ensure accurate cell trajectories. The statistics for each tracked cell were subsequently exported. To integrate both dynamic and morphological data, a custom script was developed to merge the dynamic information from TrackMate with the morphological data obtained from the µSAM segmentation labels for each individual cell. This integration was achieved by assigning the "TRACK_ID" from the TrackMate "allspots" output file to each segmented instance extracted from the TIFF file. The assignment was performed using the "measure" function in scikit-image and the KDTree distance function from the scipy module, based on the x, y, and z positions of the cells.

530 The script is available both as a downloadable version on GitHub
531 (https://github.com/imAIgene-Dream3D/MorphoTrack-merger) and as an online application
532 (https://morphotrack-merger.streamlit.app/), making this tool more accessible for non-coding
533 users.

534 **Tumor large-scale spatial phenotyping with Cytomap**

535 The positional data of various environmental surface features, segmented from LSR-3D
536 imaging data, was analyzed for large-scale spatial phenotyping using the Cytomap Spatial
537 Analysis Toolbox[44]. Briefly, neighborhoods with a 100 µm radius were generated.
538 Neighborhoods were then clustered into 2 regions based on DMG cell positioning using the
539 David Balwin algorithm. Using the gating tool, the tumor regions (containing DMG objects)
540 were defined. Next, the neighborhoods were clustered again into 3 different regions based on
541 the distribution of Iba1, Olig2, and CD31: *Void, TAMM/Oligo,* and *TAMM/vascularized*. By
542 using the *Manually Defined Regions* option, only the tumor region was classified. Finally, for
543 each region, fold-change values were calculated and exported using the *Region Statistics* tab.
544 To map the assigned regions onto IVM movies, a 3D image of the cluster distribution within
545 the tumor was generated and exported for each sample (Figure Supplement 5a). Next, regions
546 within the IVM movies were visually matched to the corresponding regions identified by the
547 Large-Scale Phenotyping module of Cytomap (Figure 3c). For each mouse, at least one or two
548 representative positions per matched region type were selected, cropped, and analyzed to assess
549 tumor cell behavior, following the previously described cell tracking methodology (*Imaris Cell*
550 *tracking*).

551 **BEHAV3D Tumor Profiler framework**

552 BEHAV3D-TP was developed using the R Studio version 4.3.3. It features three modules: 1)
553 *Heterogeneity module* with optional 2) *Large-scale and/or* 3) *Small-scale phenotyping module.*
554 These modules are described in detail below, exemplified by the analysis of DMG data from
555 this study. All of the modules are included in the same script available in Github
556 [https://github.com/imAIgene-Dream3D/BEHAV3D_Tumor_Profiler], but can be run
557 independently from one another. To acquire this independency, the optional modules are
558 directly combined to the necessary sections of the *Heterogeneity module*. Consequently, the
559 user can use whichever module is best suited for their purposes. The complete workflow—
560 combining heterogeneity analysis with large- and small-scale phenotyping—is primarily
561 optimized for datasets processed with Imaris due to its wide use in the IVM community and

special suitability for 3D visualization and tracking. In order to further facilitate public access to the BEHAV3D-TP, a Google Colab notebook has also been created accessible through the same Github page [https://github.com/imAIgene-Dream3D/BEHAV3D_Tumor_Profiler]. This environment is friendly to anyone regardless of their coding expertise as it has a step-by-step follow-through execution through the pipeline.

In addition, to broaden accessibility and support alternative data processing pipelines, the core *Heterogeneity module* of BEHAV3D-TP is also compatible with Fiji-based tracking data, specifically outputs generated by TrackMate. MTrackJ and ManualTracking. A separate Google Colab notebook is provided for these workflows on the Github page, allowing users to easily import Fiji-processed datasets, adjust analysis parameters, identify different morpho-dynamic single cell patterns.

A Wiki demo run and a video tutorial (Supplementary Video 1) are also provided through the GitHub page [https://github.com/imAIgene-Dream3D/BEHAV3D_Tumor_Profiler] for further clarification.

To ensure that your input data aligns with the workflow, we provide an online application for data quality control (https://github.com/alievakrash/BEHAV3D_TP_dataQC). This tool allows users to visualize various features, grouped by a condition of interest, and check for issues such as a high number of missing values (NA). It enables users to assess their data for any inconsistencies or unexpected patterns before proceeding with further analysis.

Heterogeneity module.

To account for missing time points and to create a time series with the same time interval for each tumor cell time series, linear interpolation was used to estimate the values of missing time points. To compare time series independently, tracks were cropped to the minimal common length among all tracks. In the case of DMG data to a 2.6 hour duration. For tracked tumor cells, time-lapse data containing the coordinates of each cell, the values of cell speed, mean square displacement, displacement delta length, displacement length, and relative distance to "Tumor edge" were used to calculate a cross-distance matrix between time series. First, we performed a principal component (PC) analysis and selected the number of PCs that explained at least 90% of data variance (3).

The previously calculated PCs were then used to compute the cross-distance matrix between each tumor cell multivariate time series using the dynamic time warping algorithm from the

593 package “dtwclust”. To visualize heterogenous tumor cell behaviors in 2 dimensions,
594 dimensionality reduction on the cross-distance matrix was performed by the Uniform Manifold
595 Approximation and Projection method (“umap” package). Clustering was performed using the
596 k-means clustering algorithm. For each cluster, the average values of distinct behavioral and
597 environmental components were calculated and plotted as a heatmap (“pheatmap”).

598 ***Large-scale phenotyping module.***

599 The information obtained from mLSR3D and Cytomap about large-scale TME regions were
600 combined with the DMG cells behavioral information (see above section *Tumor large-scale*
601 *spatial phenotyping with Cytomap)* to examine the large-scale features of tumor cells. For tumor
602 cells, the mean speed, square displacement and raw movement were analyzed.

603 ***Small-scale phenotyping module.***

604 BEHAV3D-TP enables the integration of microenvironmental features—beyond tumor cells—
605 through two distinct approaches within this module (Figure 1d). In Option 1, these
606 microenvironmental features (MEFs) are incorporated upstream and directly included in the
607 clustering process. Feature selection for this step is performed via the interface titled *"Select*
608 *the features you want to use for the environmental (morpho)-dynamic analysis."*
609 In Option 2, illustrated in Figure 4, environmental features are integrated downstream to assess
610 their correlation with pre-defined behavioral clusters. In this case, features are selected through
611 a separate interface titled *"Feature selection for projection over UMAP."*

612 In the DMG example of Figure 4 the positional coordinates of tracked tumor cells and detected
613 microenvironmental factors (TAMMs, SR101+ and blood vessels) were used to determine the
614 small-scale landscape of tumor cells. For tumor cells, the average distance to the closest 10
615 neighbors was measured to determine tumor cell density. For each tumor cell and each
616 environmental component, the number of microenvironmental objects in a 30-µm radius and
617 the distance to the closest object were computed. For each behavioral cluster, the values of
618 closest neighbors, minimal distance to each environmental factor, and number of environmental
619 objects in the 30 µm radius were plotted and compared. To quantify the percentage of DMG
620 cells in proximity to CD20r^{+} TAMMs, we classified cells located within 15 µm of TAMM
621 surfaces as “close”. For proximity to blood vessels, DMG cells were considered “close” if they
622 were within 3 µm of blood vessel spots. The difference in distance thresholds reflects the nature
623 of the reference objects: while TAMMs are defined by “Surface” boundaries, blood vessels
624 were represented by smaller centroid-based “Spots”, necessitating a more stringent cutoff.

625 **Statistical analyses**

626 Statistical analyses were performed using R. The representation of *n* may refer to individual
627 mice, distinct imaging positions within different mice, or individual cell tracks, as indicated in
628 the figure legends. Two-tailed unpaired t-tests were performed for comparison between two
629 groups in Figure supplement 1d. For comparisons involving more than two groups, where no
630 random effects were present, we performed one-way ANOVA (Figure 2d and Figure 4b),
631 followed by Tukey's Honest Significant Difference post hoc test to correct for multiple
632 comparisons. This correction was applied in Figure Supplement 4c (p-values reported in the
633 legend), as well as in Figure 3d, and Figure Supplement 5b, 5e–g. Where necessary to account
634 for inter-mouse and TME region variability, we applied a linear mixed-effects model with
635 mouse and/or TME class included as random effects (Figure 4c,e, Figure Supplement 3d, Figure
636 Supplement 6c,d). To compare the distribution of different morphodynamic clusters of TEB
637 cells, we pooled all positions and mice due to the low number of cells per position. We then
638 constructed a contingency table and performed a Chi-square test (Figure supplement 2d).

639 **Data availability**

640 DMG imaging data is publicly available at BioStudies accession number S-BIAD1759
641 (https://www.ebi.ac.uk/biostudies/studies/S-BIAD1759). Breast cancer IVM data was
642 previously described[15] and kindly provided by Dr Nienke Vrisekoop. Adult glioma IVM data
643 was previously described[7] and kindly provided by Prof. Jacco van Rhennen. Healthy breast
644 epithelium IVM was previously described[31] and kindly provided by Prof. Jane Visvader. Demo
645 outputs and Jupyter notebooks of Imaris- and Fiji-processed data are provided in our GitHib
646 repository (https://github.com/imAIgene-Dream3D/BEHAV3D_Tumor_Profiler).

647 **Code availability**

648 We provide the BEHAV3D-TP framework in a Google Colab user-friendly environment
649 [https://colab.research.google.com/drive/1JI7ysqFf3tvdi6Df4YUsSZ8RbuXw8wba?usp=shari
650 ng], as well as in an R script format in Github [https://github.com/imAIgene-
651 Dream3D/BEHAV3D_Tumor_Profiler]. Additionally, a Wiki [https://github.com/imAIgene-
652 Dream3D/BEHAV3D_Tumor_Profiler/wiki] to follow through a demo dataset as well as a
653 video tutorial (Supplementary Video 1) has been developed for further assistance. For the
654 BEHAV3D-TP heterogeneity module, we offer an online app to assess data quality
655 (https://behav3d-tp-data-qc.streamlit.app/), with the corresponding code available on GitHub
656 (https://github.com/alievakrash/BEHAV3D_TP_dataQC). Additionally, for quantifying

657 morphological features derived from Microsam segmentation and integrating them with
658 dynamic features from TrackMate, we provide another online app (https://morphotrack-
659 merger.streamlit.app/) and related code on GitHub (https://github.com/imAIgene-
660 Dream3D/MorphoTrack-merger).

661

662 **Acknowledgements**

663 We thank the Princess Máxima Center for Pediatric Oncology for technical support and the
664 Hubrecht Institute, Zeiss and the Princess Maxima Imaging Center for imaging support and
665 collaboration. We thank D. van Vuurden (Princess Máxima Center for Pediatric Oncology) and
666 Dr. Ángel Montero Carcaboso (Sant Joan de Déu Barcelona Hospital) for providing primary
667 DMG cultures; Dr Young-Tae Chang (Postech, Korea) for providing us the CD20r dye; Dr
668 Nienke Vrisekoop for sharing breast cancer IVM data; Prof. Jacco van Rheenen and Wouter
669 Beijk for sharing adult glioma IVM data; Prof Jane Visvader for sharing breast epithelial IVM
670 data; Dr Colinda Scheele and Marcel Issler for sharing healthy breast IVM data (explored but
671 not used in the current study); and members of the Dream3DLAB (Rios group) and imAIgene-
672 lab (Alieva group) for offering critical feedback on the project. A.Z. was supported by a Veni
673 fellowship from the Netherlands Organization for Scientific Research (09150161910076). R.C.
674 and A.C.R were supported by an ERC-starting grant 2018 project (no. 804412). This work was
675 produced with the support of a 2023 Leonardo Grant for Scientific Research and Cultural
676 Creation, BBVA Foundation (LEO23-2-10305-BBM-BAS-144) and the V FERO-ASEICA
677 Research Award (BFERO2024.04). M.A was supported by the Comunidad de Madrid (2022-
678 T1/BMD-24021).

679 **FIGURE LEGENDS**

680 **Fig. 1: BEHAV3D Tumor Profiler pipeline.** Schematic representation of the workflow
681 showing data preparation, input and outputs in each of the three modules. **a,** Time-lapse image
682 processing and preparation, based on segmentation and tracking of tumor (and labelled TME
683 cells). Mounting Google Drive is optional but recommended to work in the Google Colab
684 framework. **b,** Heterogeneity Module provides distinct behavioral clusters for cells, and relates
685 them to dynamic features and provides a back-projection of the tracked cells. **c, d,** Optional
686 modules, additional to the Heterogeneity module. **c,** Large-scale phenotyping module combines
687 TME large-scale information with cell morphodynamic profiling to further depict population
688 frequencies in distinct TME regions. **d,** Small-scale phenotyping module quantifies TME

689 proximity and interaction features at the single-cell level. These features can be incorporated
690 upstream as part of the clustering process to define behaviorally distinct subpopulations (option
691 1), or downstream to analyze how spatial relationships to TME components such as TAMMs
692 or vasculature vary across behavioral clusters identified in the heterogeneity module (option 2).

693 **Fig. 2: Behavioral profiling of DMG cells with BEHAV3D-TP heterogeneity module. a,**
694 Representative intravitally imaged position showing DMG cells tracked relative to tumor Edge
695 (left panel). Tracks were classified according to DMG behavior (right, color coded by cluster).
696 Representative of $n = 18$ independent positions from n=6 mice. **b,** UMAP plot showing seven
697 color-coded DMG cell behavioral clusters identified by BEHAV3D-TP. Each datapoint
698 represents one DMG cell track. A total of 981 individual cells were tracked in $n = 18$
699 independent positions from n=6 mice. **c,** Representative intravitally imaged positions and
700 enlarged sections for showcasing distinct DMG behavioral clusters *Invading* (yellow),
701 *Retreating* (green), *Erratic* (dark purple) and *Static* (light purple) through the time series. $n = 18$
702 independent positions from n=6 mice. Scale bars 10µm. **d,** Heatmap depicting relative values
703 of DMG cell features indicated for each cluster, named according to their most distinct
704 characteristics. Arbitrary units in respect to maximal and minimal values for each feature. See
705 Table 1 for features description. Bubble size according to significance levels, all features
706 represented have a significance level of $P < 0.001$ (***): *mean_displ2, mean squared*
707 *displacement; speed; delta displacement; displacement length; persistence; invasion*. P-values
708 represent the significance of differences across clusters tested through ANOVA for each
709 feature. **e, f,** UMAP representation of DMG cells' velocity relative to the tumor edge(µm) (**e**)
710 and speed (µm/h) (**f**). Each datapoint represents one cell track and is colored following a color
711 gradient. For each feature colors represent the mean DMG track values. Representative
712 of $n = 18$ independent positions from n=6 mice.

713 **Fig. 3: Mapping distinct DMG behavioral patterns to distinct TME regions. a,** Overview
714 of the large-scale TME region phenotyping workflow. After IVM imaging session, the tissue is
715 fixed and stained and then analyzed using mLSR-3D. CytoMAP Spatial Analysis Toolbox is
716 used to identify distinct large-scale regions, that are subsequently matched to IVM imaging
717 dataset (c). **b,** Representative fixed multispectral image of a mLSR3D imaged DMG tumor and
718 zoomed-in images of TME large-scale regions: *Void* (blue outline), *TAMM/vascularized* (red
719 outline) and *TAMM/Oligo* (yellow outline). DMG nuclei (blue), CD31 (pink), Olig2 (purple),
720 and Iba1 (yellow) are represented on the imaged. Scale bars, 100 µm (overview), 30 µm
721 (zoomed-in regions). **c,** 3D multispectral image DMG cell rendering color-coded per large TME

region: *Void* (blue), *TAMM/Oligo* (yellow) and *TAMM/vascularized* (red) (left). Based on the spatial coordinates of DMG cells classified into specific TME regions by CytoMAP, cells within the mLSR-3D images were subsequently assigned to their respective TME regions. Regions were then visually mapped on intravital imaging data (right). Representative of n=6 mice. White outline indicates one of the tumor regions analyzed with BEHAV3D-TP from the full tumor volume. **d** Boxplots showing the frequencies of different DMG behavioral clusters in *Void, TAMM/Oligo and TAMM/vascularized* TME large-scale regions. For each behavioral cluster, the y-axis displays the z-scored percentage of cells, normalized per mouse to account for inter-mouse variability. Each point represents an individual imaged position, with shape indicating the mouse of origin. P-values represent the significance of differences across TME regions tested through ANOVA with Tukey post hoc, for each behavioral cluster. $n = 18$ independent positions from n=6 mice.

Fig. 4: The BEHAV3D-TP small-scale phenotyping correlates DMG behavioral profiles with microenvironmental composition at a single-cell resolution. a, Overview of the small-scale TME phenotyping module. During IVM imaging, information about spatial distribution of SR101+, CD20r+, and CD31+ cells is collected and processed by the BEHAV3D-TP *small-scale phenotyping module*. Single DMG cell spatial TME features like distance to its neighbors, number of cells in a radius or minimal distance to a cell type were measured. **b,** Heatmap depicting DMG cell small-scale niches' features across distinct DMG behavioral clusters. Arbitrary units in respect to maximal and minimal values for each feature. Bubble size according to significance levels, from smallest (P < 0.05 (**)) to medium (P < 0.01 (**)) to biggest (P < 0.001 (***)): *dist_10_cell*, Distance to nearest 10 cells, P < 0.01 (**); *n*_SR101, number of SR101 cells, P < 0.05 (*); *min_SR101,* minimal distance to a SR101 cell, P < 0.05 (*); *n_CD20r,* number of CD20r cells, P < 0.05 (*); *min_Cd20r,* minimal distance to a CD20r cell, P < 0.01 (**); *min_BV_dist,* minimal distance to a Blood vessel, P < 0.001 (***). P-values represent the significance of differences across clusters tested through ANOVA for each feature. **c, e,** Boxplots depicting the percentage of DMG cells across behavioral clusters that are close to *CD20r+ TAMM* (**c**) or to *blood vessels* (**e**). Each point represents an individual imaged position, color depicts the TME large-scale region type and shape denotes the mouse. Statistical differences across clusters were assessed using a linear mixed-effects model including *mouse* and *TME class* as random effects. $P < 0.05$ (*), P < 0.01 (**), P < 0.001 (***) indicate significant differences between clusters. **c**, $n = 10$ independent positions from n=3 mice. **e**, $n = 8$ independent positions from n=3 mice. **d,** Multispectral image showing the

movement of DMG cells (grey) relative to CD20r+ TAMM (blue) and the Tumor core. The trajectories show a path from the initial (blue) to the final position (red). Scale bar, 10 µm. **f,** Time lapse multispectral images (left to right) showing the DMG cells (blue) displacement along CD31 blood vessel (purple) away from the tumor edge. Scale bars, 30 µm.

Figure supplement 1: Example application of BEHAV3D-TP for 2D movement pattern analysis of breast cancer cells tracked with MTrackJ Fiji plugin. a) Representative intravitally imaged position showing breast tumor cells tracked in 2D with the MTrackJ plugin. Red: MDA-MB-231 cells; Blue: Second Harmonic Generation; Multicolored tracks: individually tracked cells. **b)** UMAP plot showing six color-coded breast tumor cell behavioral clusters identified by BEHAV3D-TP. Each datapoint represents one cell track. A total of 935 individual cells were tracked. **c)** Heatmap depicting relative values of breast tumor cell dynamic and spatial features indicated for each cluster, named according to their most distinct characteristics. Arbitrary units in respect to maximal and minimal values for each feature. See Table 1 for features description. **d)** Boxplots showing the percentages of different breast cancer behavioral clusters for 4T1 and MDA-MB-231 cells. Each point represents a different imaging position. P-values represent the significance between both conditions measured with a Student's T test. **e)** Breast tumor cell tracks classified according to behavior (color coded by cluster in c). In all panels: representative of $n = 13$ independent positions from $n=4$ mice.

Figure supplement 2: Example application of BEHAV3D-TP for 2D morphodynamic analysis of cells segmented with CellPose2.0 and tracked using TrackMate.

a) Schematic overview of the segmentation and tracking pipeline using CellPose2.0 and TrackMate (see Methods). **b)** UMAP plot showing four color-coded morphodynamic clusters of healthy breast epithelial cells from TEBs identified by BEHAV3D-TP. Each datapoint represents one cell track. A total of 291 individual cells were tracked. **c)** Heatmap depicting relative values of epithelial cell dynamic and morphological features indicated for each cluster, named according to their most distinct characteristics. Arbitrary units in respect to maximal and minimal values for each feature. **d)** Stacked bar plot showing the distribution of morphodynamic cell types across the two indicated TEB populations: HR+ luminal progenitor cells and HR− luminal progenitor cells. Combined data from 19 mice and 72 independent positions. Chi-square test indicates p=0.02 for cluster 2.

Figure supplement 3: Example application of BEHAV3D-TP for 3D morphodynamic analysis of cells segmented with µSAM and tracked using TrackMate.

787 **a)** Schematic overview of the segmentation and tracking pipeline using µSAM and TrackMate.
788 An online app was developed to integrate morphological and dynamic features (see Methods).
789 **b)** UMAP plot showing four color-coded morphodynamic clusters of GBM cells identified by
790 BEHAV3D-TP. Each datapoint represents one cell track. Total of 460 individually tracked
791 cells. **c)** Heatmap depicting relative values of GBM cell dynamic and morphological features
792 indicated for each cluster, named according to their most distinct characteristics. Arbitrary units
793 in respect to maximal and minimal values for each feature. See Table 1 for features description.
794 **d)** Boxplot showing *Average distance to the 3 closest GBM neighbors (pixels)* across distinct
795 GBM morphodynamic clusters. Each data point represents the per-mouse average, calculated
796 from a total of six independent imaging positions. Statistical significance across behavioral
797 clusters was assessed using a linear mixed model with mouse as a random effect. $P < 0.05$ (*).

798 **Figure supplement 4: DMG cells heterogeneity captured by intravital imaging. a,**
799 Schematic representation of an intravital imaging experimental design, capturing timelapses up
800 to 5.4 hours of DMG cells expressing H2BmNeonGreen and mScarlet proteins, followed by
801 single-cell tracking. **b,** Representative intravitally imaged position showing DMG cell tracks
802 colored by behavioral cluster projected over the last timepoint of the original IVM time-lapse.
803 **c,** Quantification of average DMG cell speed (µm/h) in each identified behavioral cluster per
804 mouse. Significance of differences across behavioral clusters tested through ANOVA followed
805 by Tukey's post hoc test. All comparisons significant, except cluster 5-2, 4-7, 1-6, 7-3, 3-6, 3-
806 4 and 6-4. **d,** Behavioral cluster frequency distribution across individual IVM imaged mice.
807 (c,d) Each data point represents the average per mouse, computed from 18 independent imaging
808 positions.

809 **Figure supplement 5: Cell type and behavioral cluster frequency distribution in identified**
810 **TME large-scale regions. a,** Representative CytoMap output showcasing**,** 3D spatial
811 distribution of DMG cells in distinct TME large-scale regions: *Void* (blue), *TAMM/Oligo*
812 (yellow) and *TAMM/vascularized* (red). Each datapoint represent a unique DMG cell within a
813 classified large-scale region. **b, c,** Fold change of cell count of DMG, Iba1+, Olig2+ and CD31+
814 cell types, identified with mLSR3D fixed imaging, relative to the mean cell count in each TME
815 large scale region (*Void, TAMM/Oligo, TAMM/vascularized)*, both in boxplot (**b**) and table (**c**)
816 formats. In **(b)** each point represents a mouse, n=7. For DMG cell count: *TAMM/Oligo* versus
817 *Void,* P < 0.01 (**); *TAMM/Oligo* versus *TAMM/vascularized*, P < 0.05 (*). For Iba1 cell count:
818 *TAMM/Oligo* versus *Void*, P < 0.001 (***); *TAMM/vascularized* versus *Void*, P < 0.001 (***).
819 In Olig2 cell count: *TAMM/Oligo* versus *Void,* P < 0.001 (***); *TAMM/Oligo* versus

820 *TAMM/vascularized*, P < 0.001 (***). For CD31 cell count: *TAMM/Oligo* versus *Void,* P <
821 0.001 (***); *TAMM/vascularized* versus *Void,* P < 0.001 (***); *TAMM/Oligo* versus
822 *TAMM/vascularized*, P < 0.001 (***). **d,** Boxplots showing the percentages of different DMG
823 behavioral clusters in *Void, TAMM/Oligo and TAMM/vascularized* TME large-scale regions.
824 Each point represents a different imaging position. Color: *n* = 18 independent positions; Shape:
825 *n*=6 mice. **e, f, g,** Boxplots plots showing DMG single cell features (*Tumor cell speed*
826 (µm/hour) (**e**), *Average speed displacement* (**f**) *and Tumor cell velocity* (µm/hour) (**g**))
827 differences among *Void, TAMM/Oligo and TAMM/vascularized* per mouse in TME large-scale
828 regions. **g,** Tumor cell velocity can be either towards brain core (down, negative values) or
829 towards brain parenchyma (up, positive values). For **e, f, g:** Each data point represents the
830 average per mouse, computed from 18 independent imaging positions. Statistical differences
831 were assessed using one-way ANOVA. No statistically significant differences were found.

832 **Figure supplement 6: Cell distribution and behavioral clusters in small-scale TME. a, b,**
833 Representative 3D IVM rendering of *DMG nuclei* (cyan), CD31+ cells (grey) and SR101+ (**a**,
834 red) or CD20r+ cells (**b**, red). Scale bars, 100 µm. **c, d,** Boxplots showing *Average distance to*
835 *the 10 closest DMG neighbors (µm)* (**c**) and *Number of SR101+ cells in a 30 µm radius* (**d**)
836 across distinct DMG single-cell behavioral clusters. (**c)** Each point represents an individual
837 mouse. Statistical differences across clusters were assessed using a linear mixed-effects model
838 including *mouse* as random effect. *P* < 0.05 (*) indicate significant differences between clusters.
839 *n* =18 independent positions from *n*=6 mice. **(d)** Each point represents an individual imaged
840 position, color depicts the TME large-scale region type and shape denotes the mouse. Statistical
841 differences across clusters were assessed using a linear mixed-effects model including *mouse*
842 and *TME class* as random effects. *P* < 0.05 (*), P < 0.01 (**) indicate significant differences
843 between clusters. *n*=8 independent positions from *n*=3 mice.

844 **Supplementary video 1: BEHAV3D Tumor Profiler pipeline main characteristics and**
845 **walkthrough**. Summary video of BEHAV3D TP pipeline.

846 **Supplementary video 2: Representative intravital time-lapse video of DMG cells.** Raw
847 DMG cells time-lapse (right panel). Cell tracks were classified according to DMG behavior
848 (right panel, color coded by cluster). Representative movie from n=18 independent positions
849 imaged in 6 mice. Scale bars 40 µm.

850 **Supplementary video 3: Dynamic multispectral representative time-lapse video of DMG**
851 **cells and CD20r+ TAMM.** Time-lapse showing the movement of DMG cells (grey) relative

852 to CD20r+ TAMM (blue). The trajectories towards the TAMM of two DMG cells show a path
853 from the initial (blue) to the final position (red). Left: Tumor edge; right: tumor core.
854 Representative movie from n=10 independent positions imaged in 3 mice. Scale bars 10 µm, 7
855 µm after zoom in.

856

857 **REFERENCES**
858

859 1. Vitale, I., Shema, E., Loi, S. & Galluzzi, L. Intratumoral heterogeneity in cancer progression and
860 response to immunotherapy. *Nat Med* **27**, 212–224 (2021).

861 2. Lawson, D. A., Kessenbrock, K., Davis, R. T., Pervolarakis, N. & Werb, Z. Tumour heterogeneity
862 and metastasis at single-cell resolution. *Nat. Cell Biol.* **20**, 1349–1360 (2018).

863 3. Elhanani, O., Ben-Uri, R. & Keren, L. Spatial profiling technologies illuminate the tumor microen-
864 vironment. *Cancer Cell* **41**, 404–420 (2023).

865 4. Scheele, C. L. G. J., Maynard, C. & Rheenen, J. van. Intravital Insights into Heterogeneity, Metasta-
866 sis, and Therapy Responses. *Trends Cancer* **2**, 205–216 (2016).

867 5. Entenberg, D., Oktay, M. H. & Condeelis, J. S. Intravital imaging to study cancer progression and
868 metastasis. *Nat. Rev. Cancer* **23**, 25–42 (2023).

869 6. Alieva, M., Ritsma, L., Giedt, R. J., Weissleder, R. & Rheenen, J. van. Imaging windows for long-
870 term intravital imaging. *IntraVital* **3**, e29917 (2014).

871 7. Alieva, M. *et al.* Intravital imaging of glioma border morphology reveals distinctive cellular dynam-
872 ics and contribution to tumor cell invasion. *Sci. Rep.* **9**, 2054 (2019).

873 8. Alieva, M. & Rios, A. C. Longitudinal Intravital Imaging of Brain Tumor Cell Behavior in Re-
874 sponse to an Invasive Surgical Biopsy. *J. Vis. Exp.* (2019) doi:10.3791/59278.

875 9. Zomer, A., Croci, D., Kowal, J., Gurp, L. van & Joyce, J. A. Multimodal imaging of the dynamic
876 brain tumor microenvironment during glioblastoma progression and in response to treatment. *iScience*
877 **25**, 104570 (2022).

878 10. Alieva, M. *et al.* Preventing inflammation inhibits biopsy-mediated changes in tumor cell behav-
879 ior. *Sci. Rep.* **7**, 7529 (2017).

880 11. Janssen, A., Beerling, E., Medema, R. & Rheenen, J. van. Intravital FRET Imaging of Tumor Cell
881 Viability and Mitosis during Chemotherapy. *PLoS ONE* **8**, e64029 (2013).

882 12. Croci, D., Zomer, A., Kowal, J. & Joyce, J. A. Cranial imaging window implantation technique
883 for longitudinal multimodal imaging of the brain environment in live mice. *STAR Protoc.* **4**, 102197
884 (2023).

885 13. Zomer, A. *et al.* Brief Report: Intravital Imaging of Cancer Stem Cell Plasticity in Mammary Tu-
886 mors. *STEM CELLS* **31**, 602–606 (2013).

887 14. Zomer, A. *et al.* In Vivo Imaging Reveals Extracellular Vesicle-Mediated Phenocopying of Meta-
888 static Behavior. *Cell* **161**, 1046–1057 (2015).

889 15. Chen, N., Ritsma, L. M. A. & Vrisekoop, N. In vivo characteristics of human and mouse breast
890 tumor cell lines. *Exp. Cell Res.* **381**, 86–93 (2019).

891 16. Bayarmagnai, B., Perrin, L., Pourfarhangi, K. E. & Gligorijevic, B. Cell Migration, Methods and
892 Protocols. *Methods Mol. Biol.* **1749**, 175–193 (2018).

17. Shannon, M. J., Eisman, S. E., Lowe, A. R., Sloan, T. & Mace, E. M. cellPLATO: an unsupervised method for identifying cell behaviour in heterogeneous cell trajectory data. *J. Cell Sci.* **137**, jcs261887.

18. Crainiciuc, G. *et al.* Behavioural immune landscapes of inflammation. *Nature* **601**, 415–421 (2022).

19. Dekkers, J. F. *et al.* Uncovering the mode of action of engineered T cells in patient cancer organoids. *Nat. Biotechnol.* **41**, 60–69 (2023).

20. Freckmann, E. C. *et al.* Traject3d allows label-free identification of distinct co-occurring phenotypes within 3D culture by live imaging. *Nat. Commun.* **13**, 5317 (2022).

21. Alieva, M. *et al.* BEHAV3D: a 3D live imaging platform for comprehensive analysis of engineered T cell behavior and tumor response. *Nat. Protoc.* 1–33 (2024) doi:10.1038/s41596-024-00972-6.

22. Pizzagalli, D. U. *et al.* Leukocyte Tracking Database, a collection of immune cell tracks from intravital 2-photon microscopy videos. *Sci. Data* **5**, 180129 (2018).

23. Pizzagalli, D. U. *et al.* CANCOL, a Computer-Assisted Annotation Tool to Facilitate Colocalization and Tracking of Immune Cells in Intravital Microscopy. *J. Immunol.* **208**, 1493–1499 (2022).

24. Joseph, A., Chu, C. J., Feng, G., Dholakia, K. & Schallek, J. Label-free imaging of immune cell dynamics in the living retina using adaptive optics. *eLife* **9**, e60547 (2020).

25. Molina-Moreno, M. *et al.* ACME: Automatic feature extraction for cell migration examination through intravital microscopy imaging. *Méd. Image Anal.* **77**, 102358 (2022).

26. Hidalgo-Cenalmor, I. *et al.* DL4MicEverywhere: deep learning for microscopy made flexible, shareable and reproducible. *Nat. Methods* **21**, 925–927 (2024).

27. Ershov, D. *et al.* TrackMate 7: integrating state-of-the-art segmentation algorithms into tracking pipelines. *Nat Methods* **19**, 829–832 (2022).

28. Buczkowicz, P., Bartels, U., Bouffet, E., Becher, O. & Hawkins, C. Histopathological spectrum of paediatric diffuse intrinsic pontine glioma: diagnostic and therapeutic implications. *Acta Neuropathol.* **128**, 573–581 (2014).

29. Gómez-de-Mariscal, E. *et al.* CellTracksColab — A platform for compiling, analyzing, and exploring tracking data. *bioRxiv* 2023.10.20.563252 (2024) doi:10.1101/2023.10.20.563252.

30. Chamier, L. von *et al.* Democratising deep learning for microscopy with ZeroCostDL4Mic. *Nat Commun* **12**, 2276 (2021).

31. Dawson, C. A. *et al.* Hormone-responsive progenitors have a unique identity and exhibit high motility during mammary morphogenesis. *Cell Rep.* **43**, 115073 (2024).

32. Pachitariu, M. & Stringer, C. Cellpose 2.0: how to train your own model. *Nat. Methods* **19**, 1634–1641 (2022).

33. Archit, A. *et al.* Segment Anything for Microscopy. *Nat. Methods* **22**, 579–591 (2025).

928 34. Dawson, C. A., Mueller, S. N., Lindeman, G. J., Rios, A. C. & Visvader, J. E. Intravital micros-
929 copy of dynamic single-cell behavior in mouse mammary tissue. *Nat. Protoc.* **16**, 1907–1935 (2021).

930 35. Jung, E. *et al.* Tumor cell plasticity, heterogeneity, and resistance in crucial microenvironmental
931 niches in glioma. *Nat. Commun.* **12**, 1014 (2021).

932 36. Crainiciuc, G. *et al.* Behavioural immune landscapes of inflammation. *Nature* 1–7 (2022)
933 doi:10.1038/s41586-021-04263-y.

934 37. Jarade, A. *et al.* Inflammation triggers ILC3 patrolling of the intestinal barrier. *Nat. Immunol.* **23**,
935 1317–1323 (2022).

936 38. Chauveau, A. *et al.* Visualization of T Cell Migration in the Spleen Reveals a Network of Peri-
937 vascular Pathways that Guide Entry into T Zones. *Immunity* **52**, 794-807.e7 (2020).

938 39. Kienle, K. *et al.* Neutrophils self-limit swarming to contain bacterial growth in vivo. *Science* **372**,
939 (2021).

940 40. Liu, B. *et al.* Affinity-coupled CCL22 promotes positive selection in germinal centres. *Nature* **592**,
941 133–137 (2021).

942 41. Persson, M. L. *et al.* The intrinsic and microenvironmental features of diffuse midline glioma: Im-
943 plications for the development of effective immunotherapeutic treatment strategies. *Neuro-Oncol.* **24**,
944 1408–1422 (2022).

945 42. Ineveld, R. L. van *et al.* Multispectral confocal 3D imaging of intact healthy and tumor tissue us-
946 ing mLSR-3D. *Nat. Protoc.* **17**, 3028–3055 (2022).

947 43. Ineveld, R. L. van *et al.* Revealing the spatio-phenotypic patterning of cells in healthy and tumor
948 tissues with mLSR-3D and STAPL-3D. *Nat. Biotechnol.* **39**, 1239–1245 (2021).

949 44. Stoltzfus, C. R. *et al.* CytoMAP: A Spatial Analysis Toolbox Reveals Features of Myeloid Cell
950 Organization in Lymphoid Tissues. *Cell Rep.* **31**, 107523 (2020).

951 45. Winkler, F. *et al.* Imaging glioma cell invasion in vivo reveals mechanisms of dissemination and
952 peritumoral angiogenesis. *Glia* **57**, 1306–1315 (2009).

953 46. Wallmann, T. *et al.* Microglia Induce PDGFRB Expression in Glioma Cells to Enhance Their Mi-
954 gratory Capacity. *iScience* **9**, 71–83 (2018).

955 47. Seano, G. & Jain, R. K. Vessel co-option in glioblastoma: emerging insights and opportunities. *An-*
956 *giogenesis* **23**, 9–16 (2020).

957 48. Ravin, R. *et al.* Perivascular invasion of primary human glioblastoma cells in organotypic human
958 brain slices: human cells migrating in human brain. *J. Neuro-Oncol.* **164**, 43–54 (2023).

959 49. Gupta, R. K. *et al.* Tumor-specific migration routes of xenotransplanted human glioblastoma cells
960 in mouse brain. *Sci. Rep.* **14**, 864 (2024).

961 50. Nimmerjahn, A., Kirchhoff, F., Kerr, J. N. D. & Helmchen, F. Sulforhodamine 101 as a specific
962 marker of astroglia in the neocortex in vivo. *Nat. Methods* **1**, 31–37 (2004).

963 51. Appaix, F. *et al.* Specific In Vivo Staining of Astrocytes in the Whole Brain after Intravenous In-
964 jection of Sulforhodamine Dyes. *PLoS ONE* **7**, e35169 (2012).

965 52. Rasmussen, R., Nedergaard, M. & Petersen, N. C. Sulforhodamine 101, a widely used astrocyte
966 marker, can induce cortical seizure-like activity at concentrations commonly used. *Sci. Rep.* **6**, 30433
967 (2016).

968 53. Hagos, L. & Hülsmann, S. Unspecific labelling of oligodendrocytes by sulforhodamine 101 de-
969 pends on astrocytic uptake via the thyroid hormone transporter OATP1C1 (SLCO1C1). *Neurosci. Lett.*
970 **631**, 13–18 (2016).

971 54. Kim, B. *et al.* Visualizing Microglia with a Fluorescence Turn-On Ugt1a7c Substrate. *Angew.*
972 *Chem. Int. Ed.* **58**, 7972–7976 (2019).

973 55. Liu, I. *et al.* The landscape of tumor cell states and spatial organization in H3-K27M mutant dif-
974 fuse midline glioma across age and location. *Nat. Genet.* **54**, 1881–1894 (2022).

975 56. Xin, T. *et al.* Oncogenic Kras induces spatiotemporally specific tissue deformation through con-
976 verting pulsatile into sustained ERK activation. *Nat. Cell Biol.* **26**, 859–867 (2024).

977 57. Venkataramani, V. *et al.* Glioblastoma hijacks neuronal mechanisms for brain invasion. *Cell* **185**,
978 2899-2917.e31 (2022).

979 58. Bera, K. *et al.* Extracellular fluid viscosity enhances cell migration and cancer dissemination. *Na-*
980 *ture* **611**, 365–373 (2022).

981 59. Gertler, F. & Condeelis, J. Metastasis: tumor cells becoming MENAcing. *Trends Cell Biol.* **21**,
982 81–90 (2011).

983 60. Kluiver, T. A., Alieva, M., Vuurden, D. G. van, Wehrens, E. J. & Rios, A. C. Invaders Exposed:
984 Understanding and Targeting Tumor Cell Invasion in Diffuse Intrinsic Pontine Glioma. *Front. Oncol.*
985 **10**, 92 (2020).

986 61. Quail, D. F. & Joyce, J. A. The Microenvironmental Landscape of Brain Tumors. *Cancer Cell* **31**,
987 326–341 (2017).

988 62. Taylor, K. R. & Monje, M. Invasive glioma cells: The malignant pioneers that follow the current.
989 *Cell* **185**, 2846–2848 (2022).

990 63. Erices, J. I. *et al.* Glioblastoma Microenvironment and Invasiveness: New Insights and Therapeutic
991 Targets. *Int. J. Mol. Sci.* **24**, 7047 (2023).

992 64. Patel, S. K. *et al.* Generation of diffuse intrinsic pontine glioma mouse models by brainstem-tar-
993 geted in utero electroporation. *Neuro-Oncol.* **22**, 381–392 (2020).

994 65. Chatinier, A. du *et al.* Generation of immunocompetent syngeneic allograft mouse models for pe-
995 diatric diffuse midline glioma. *Neuro-Oncol. Adv.* **4**, vdac079 (2022).

996 66. Srivastava, R. *et al.* Development of a human glioblastoma model using humanized DRAG mice
997 for immunotherapy. *Antib. Ther.* **6**, 253–264 (2023).

998 67. Wezenaar, A. K. L. *et al.* Mapping T cell dynamics to molecular profiles through behavior-guided
999 transcriptomics. *Nat. Protoc.* 1–28 (2025) doi:10.1038/s41596-024-01126-4.

1000 68. Aragones, D. G. *et al.* Variable selection for nonlinear dimensionality reduction of biological da-
1001 tasets through bootstrapping of correlation networks. *Comput. Biol. Med.* **168**, 107827 (2024).

1002 69. Klein, S., Staring, M., Murphy, K., Viergever, M. A. & Pluim, J. P. W. elastix: A Toolbox for In-
1003 tensity-Based Medical Image Registration. *IEEE Trans. Méd. Imaging* **29**, 196–205 (2010).

1004 70. Marstal, K., Berendsen, F., Staring, M. & Klein, S. SimpleElastix: A User-Friendly, Multi-Lingual
1005 Library for Medical Image Registration. *2016 IEEE Conf. Comput. Vis. Pattern Recognit. Work.*
1006 *(CVPRW)* 574–582 (2016) doi:10.1109/cvprw.2016.78.

1007 71. Rios, A. C. *et al.* Intraclonal Plasticity in Mammary Tumors Revealed through Large-Scale Single-
1008 Cell Resolution 3D Imaging. *Cancer Cell* **35**, 618-632.e6 (2019).

1009

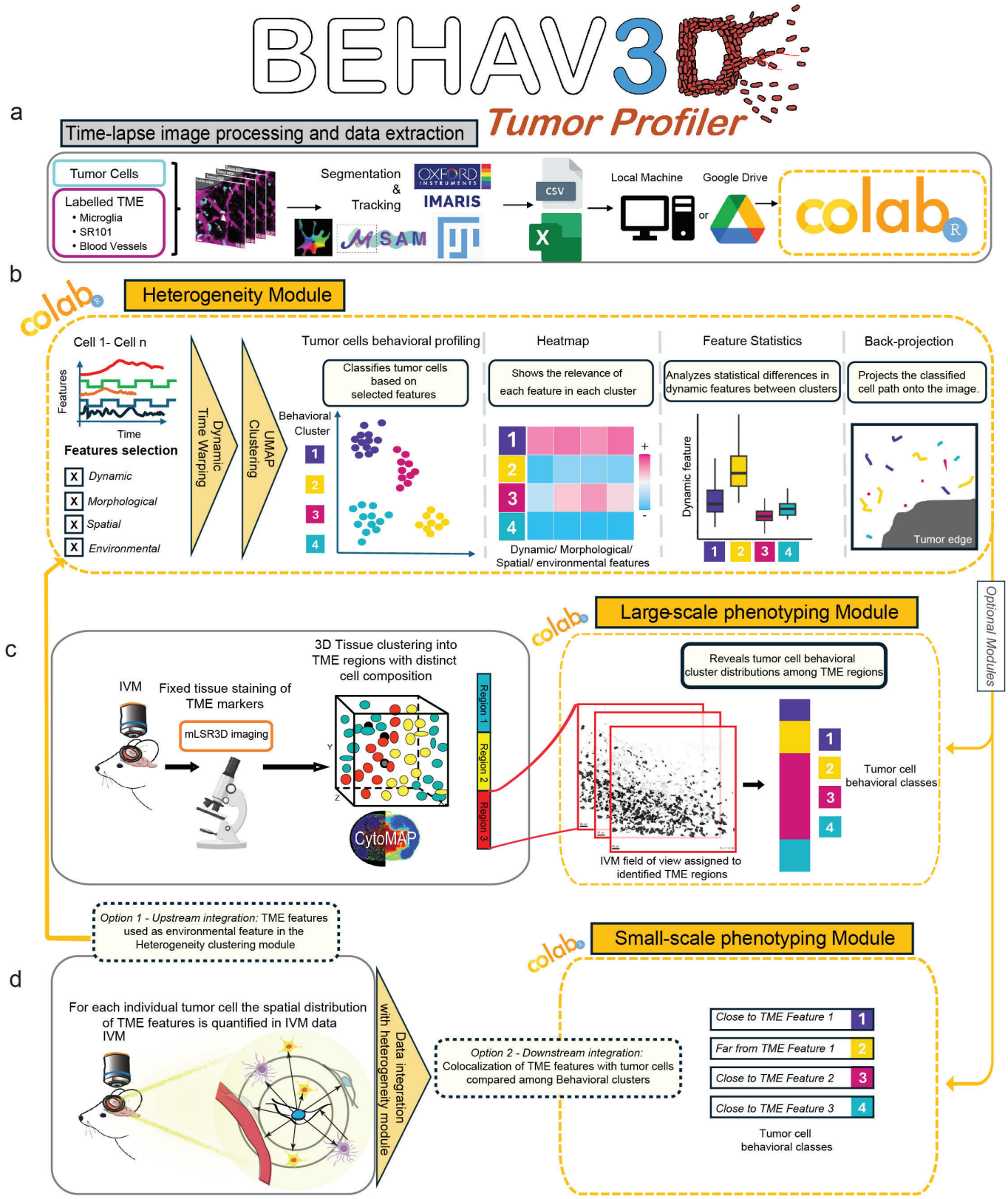
BEHAV3D
Tumor Profiler
a
Time-lapse image processing and data extraction
Tumor Cells
Labelled TME
• Microglia
• SR101
• Blood Vessels
Segmentation & Tracking
OXFORD INSTRUMENTS
IMARIS
MSAM
CSV
Local Machine
Google Drive
or
colab
b
Heterogeneity Module
Cell 1- Cell n
Features
Time
Features selection
X Dynamic
X Morphological
X Spatial
X Environmental
Dynamic Time Warping
UMAP Clustering
Tumor cells behavioral profiling
Classifies tumor cells based on selected features
Behavioral Cluster
1
2
3
4
Heatmap
Shows the relevance of each feature in each cluster
Dynamic/ Morphological/ Spatial/ environmental features
Feature Statistics
Analyzes statistical differences in dynamic features between clusters
Dynamic feature
Back-projection
Projects the classified cell path onto the image.
Tumor edge
Optional Modules
c
Large-scale phenotyping Module
IVM
Fixed tissue staining of TME markers
mLSR3D imaging
3D Tissue clustering into TME regions with distinct cell composition
Region 1
Region 2
Region 3
CytoMAP
Reveals tumor cell behavioral cluster distributions among TME regions
IVM field of view assigned to identified TME regions
Tumor cell behavioral classes
Option 1 - Upstream integration: TME features used as environmental feature in the Heterogeneity clustering module
d
Small-scale phenotyping Module
For each individual tumor cell the spatial distribution of TME features is quantified in IVM data
IVM
Data integration with heterogeneity module
Option 2 - Downstream integration: Colocalization of TME features with tumor cells compared among Behavioral clusters
Close to TME Feature 1
Far from TME Feature 1
Close to TME Feature 2
Close to TME Feature 3
Tumor cell behavioral classes

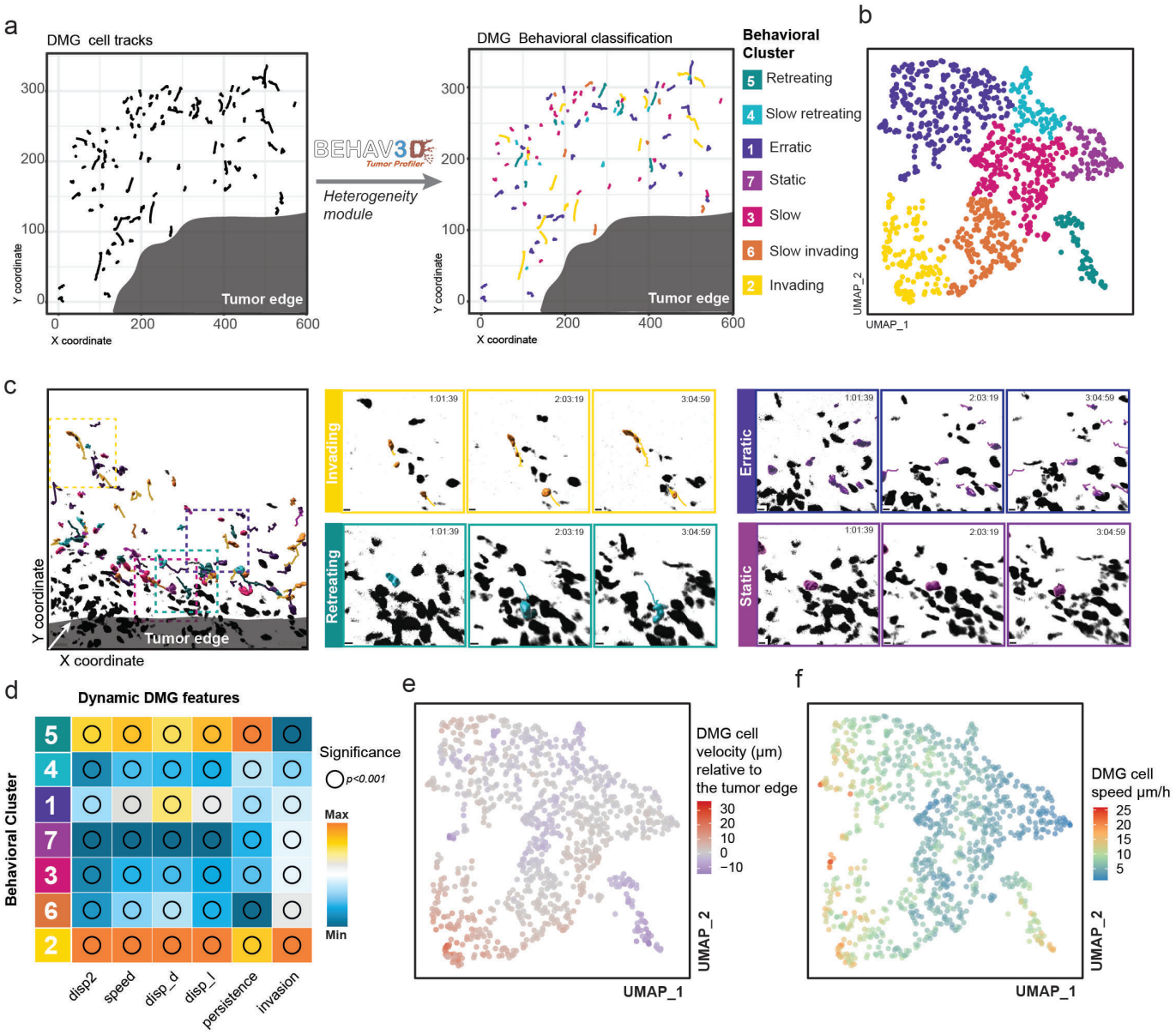

Figure 2. Behavioral profiling of DMG cells with BEHAV3D-TP heterogeneity module.

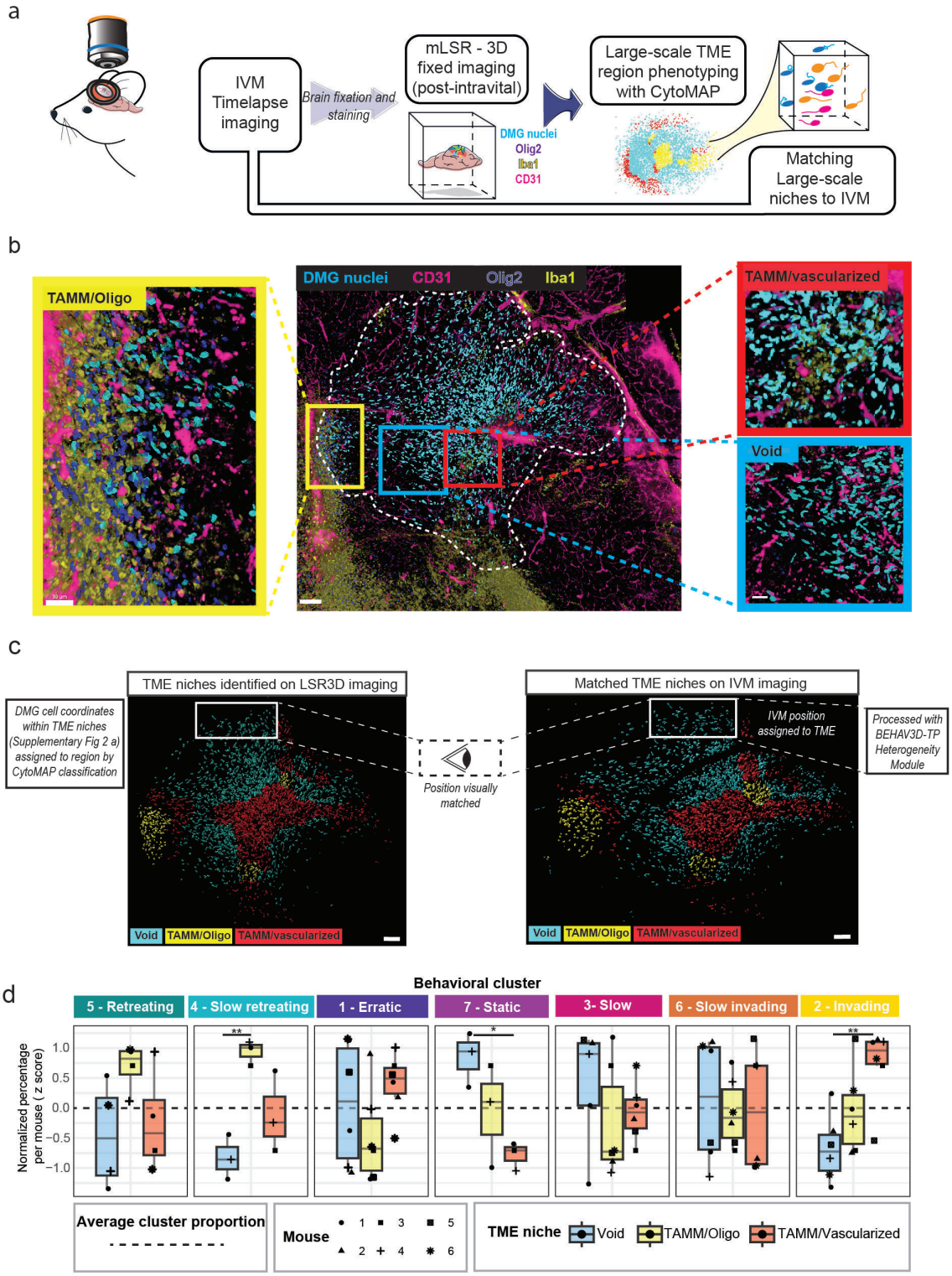

Figure 3: Mapping distinct DMG behavioral patterns to distinct TME regions

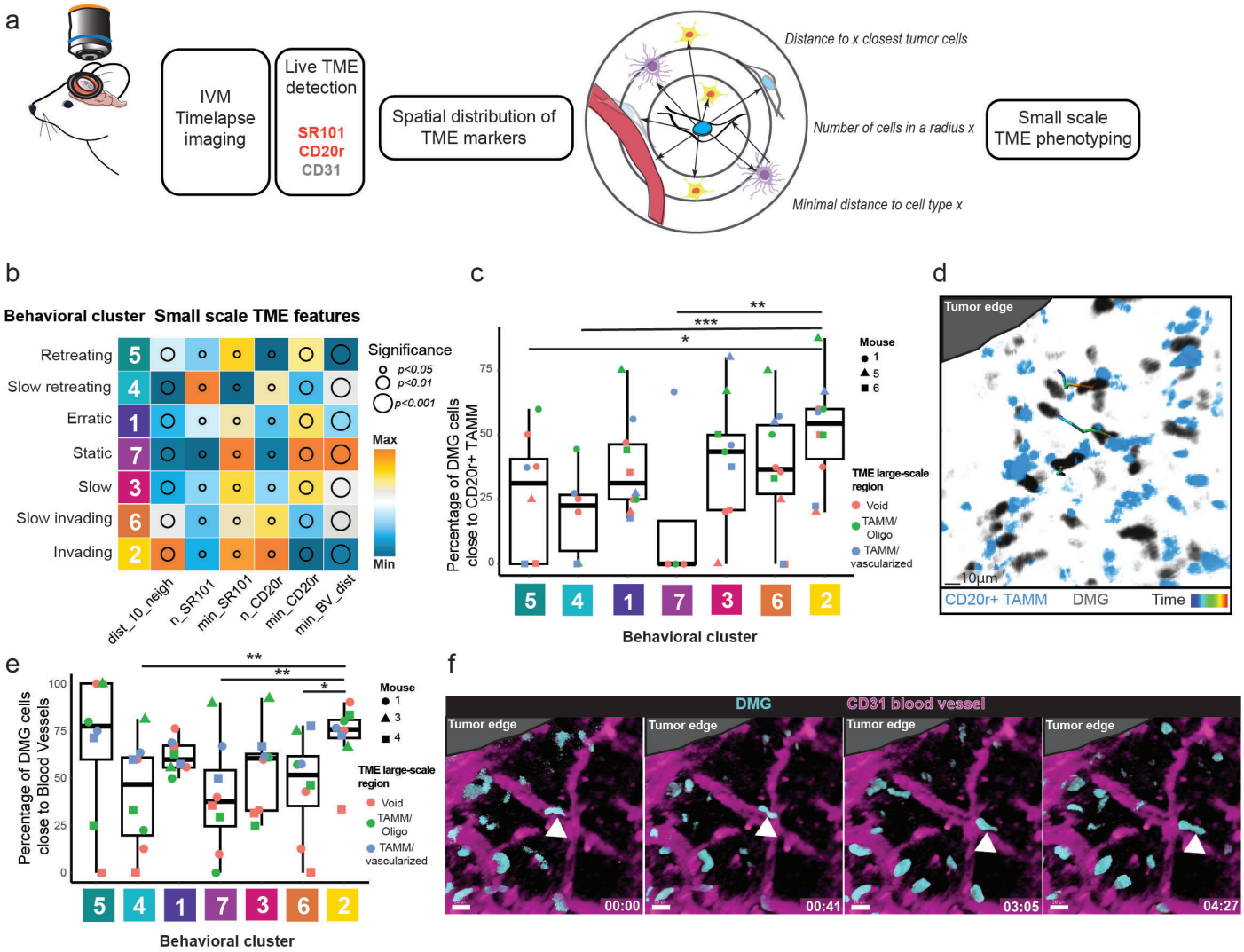

Figure 4. The BEHAV3D-TP small-scale phenotyping correlates DMG behavioral profiles with microenvironmental composition at a single-cell resolution

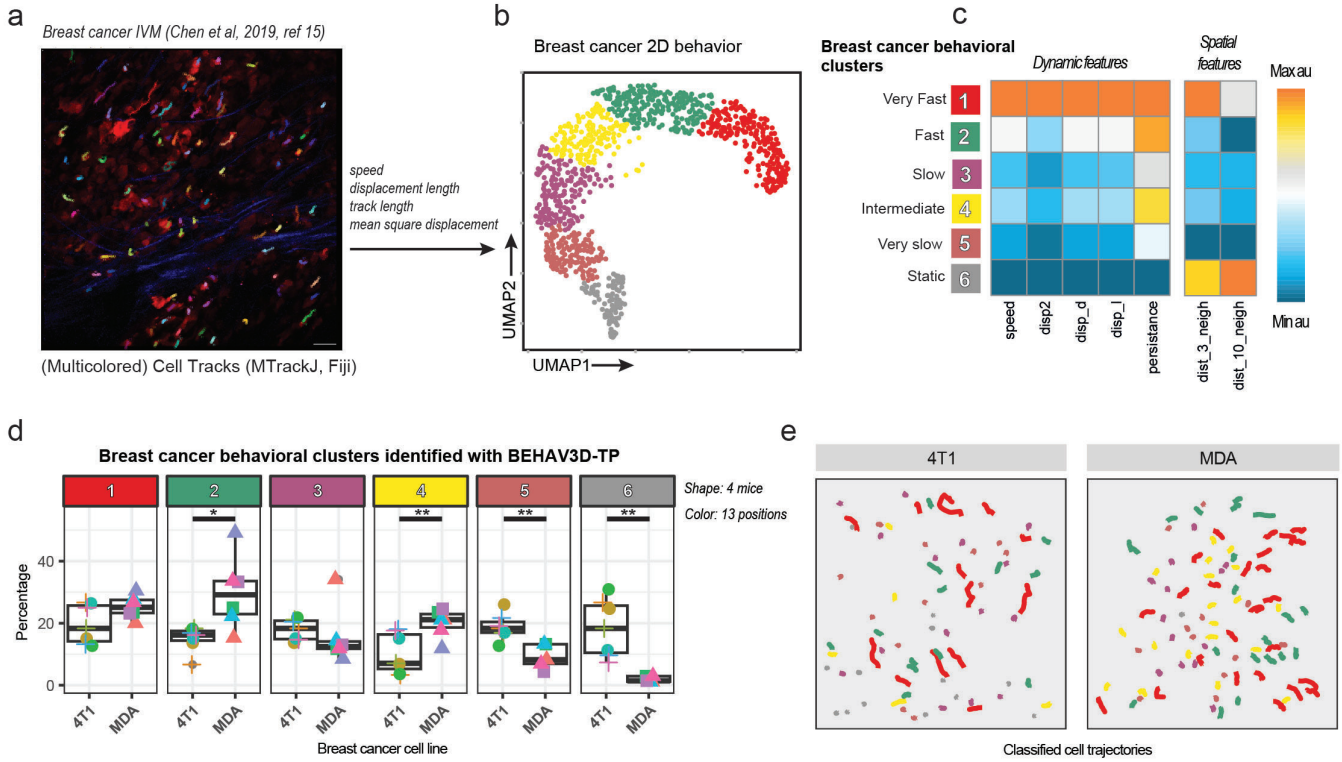

Supplementary Figure 1: Example application of BEHAV3D-TP for 2D movement pattern analysis of breast cancer cells tracked with MTrackJ Fiji plugin.

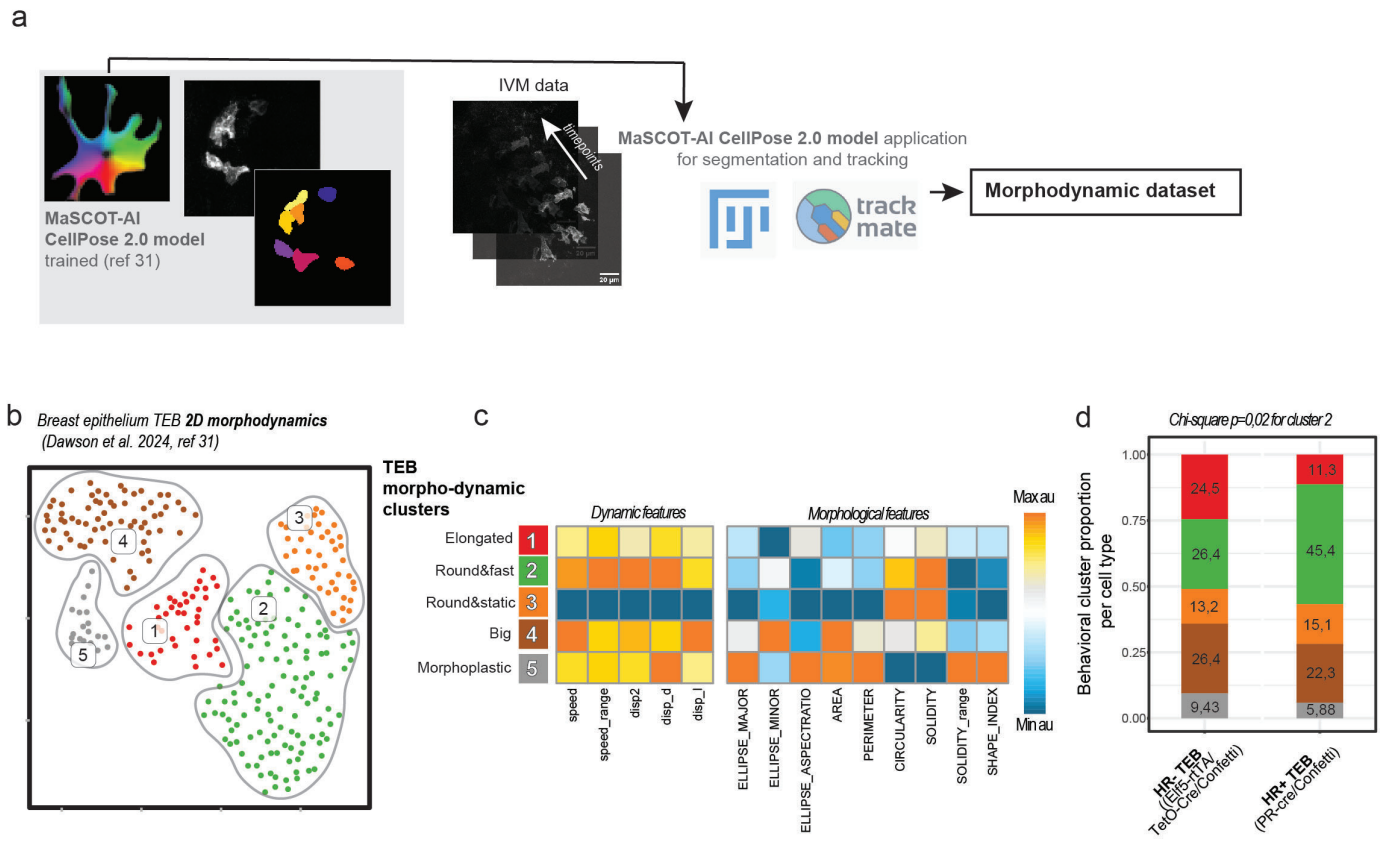

Supplementary Figure 2: Example application of BEHAV3D-TP for 2D morphodynamic analysis of cells segmented with CellPose2.0 and tracked using TrackMate

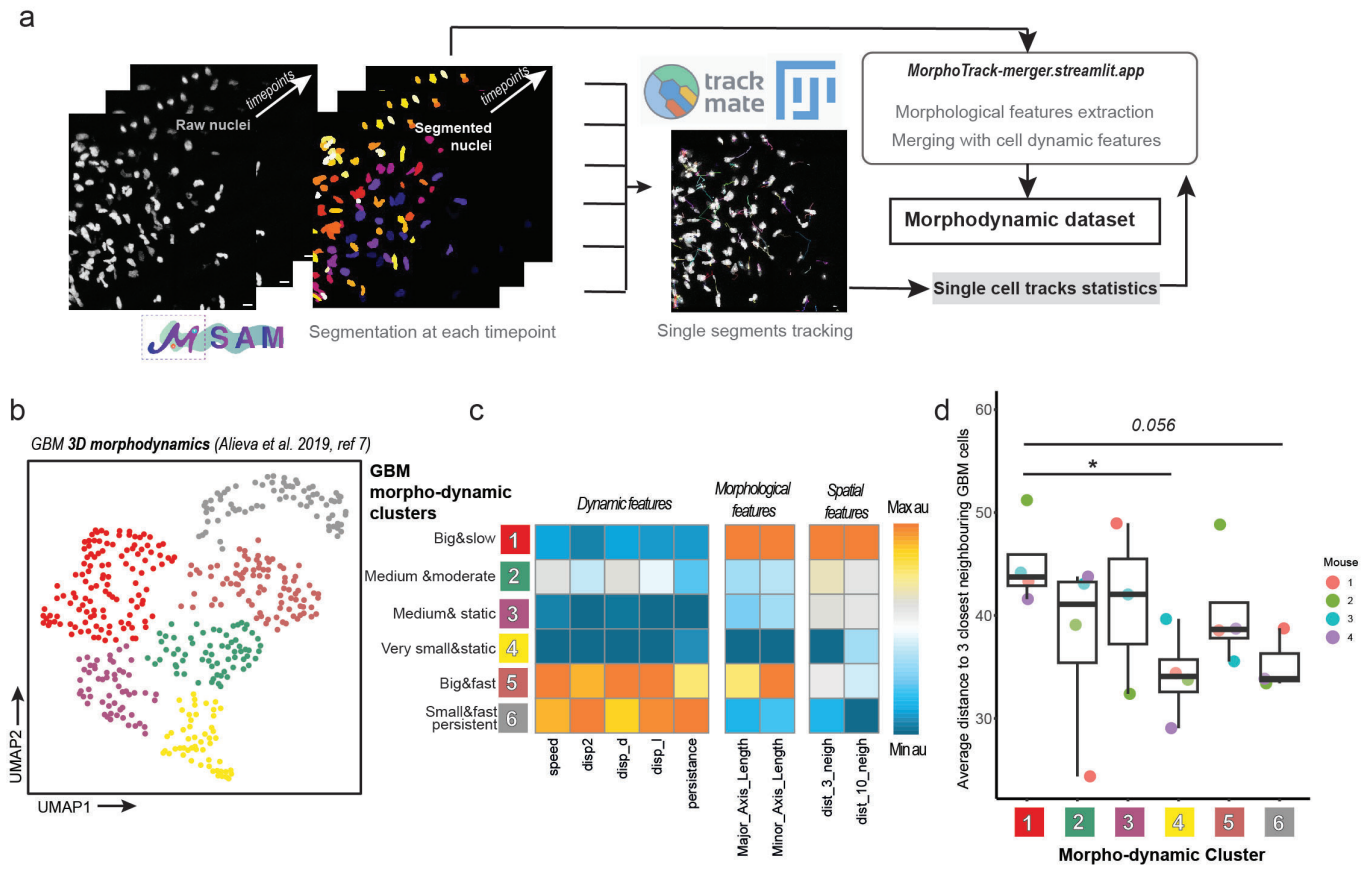

Supplementary Figure 3: Example application of BEHAV3D-TP for 3D morphodynamic analysis of cells segmented with μSAM and tracked using TrackMate

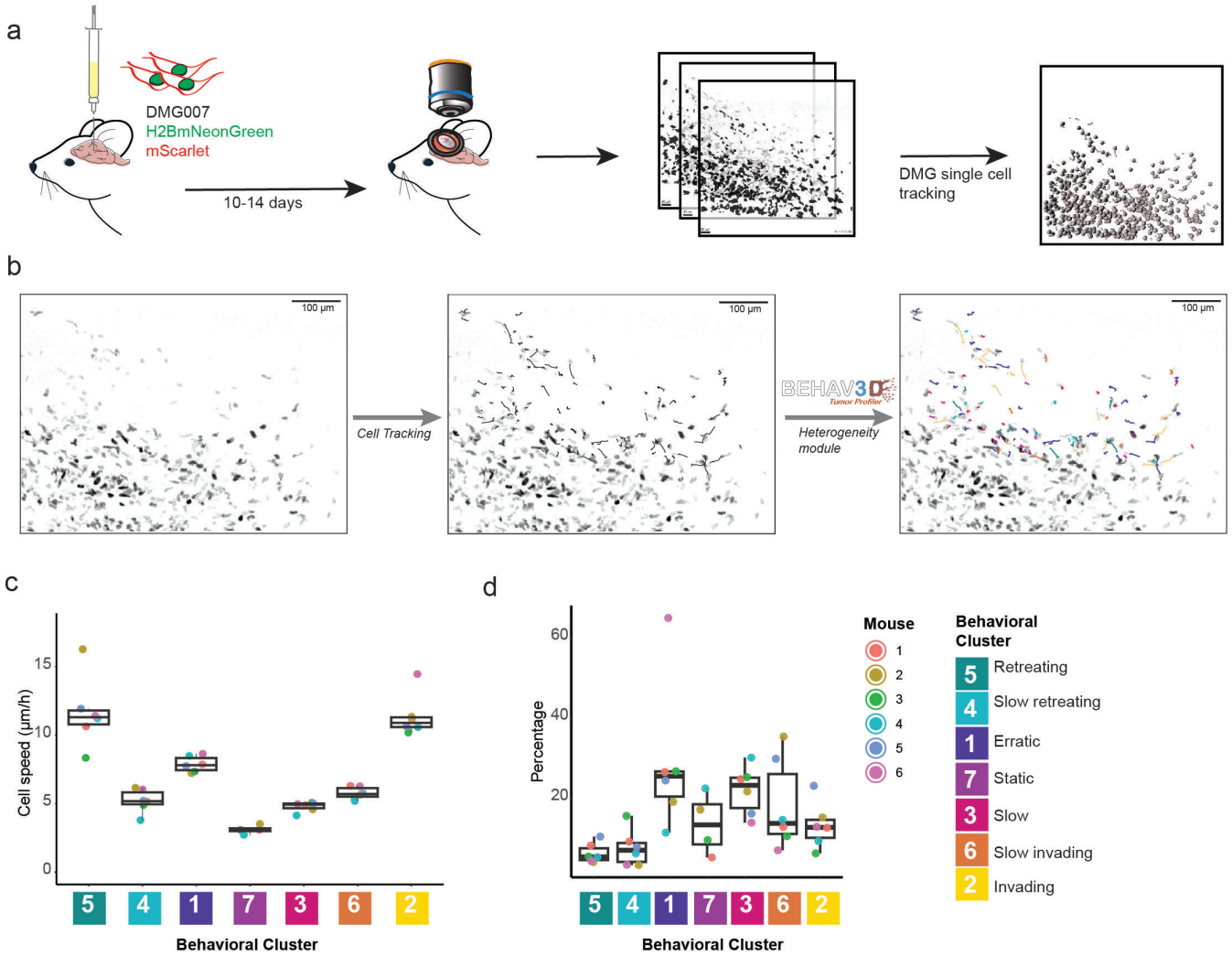

Supplementary Figure 4. DMG cells heterogeneity captured by intravital imaging.

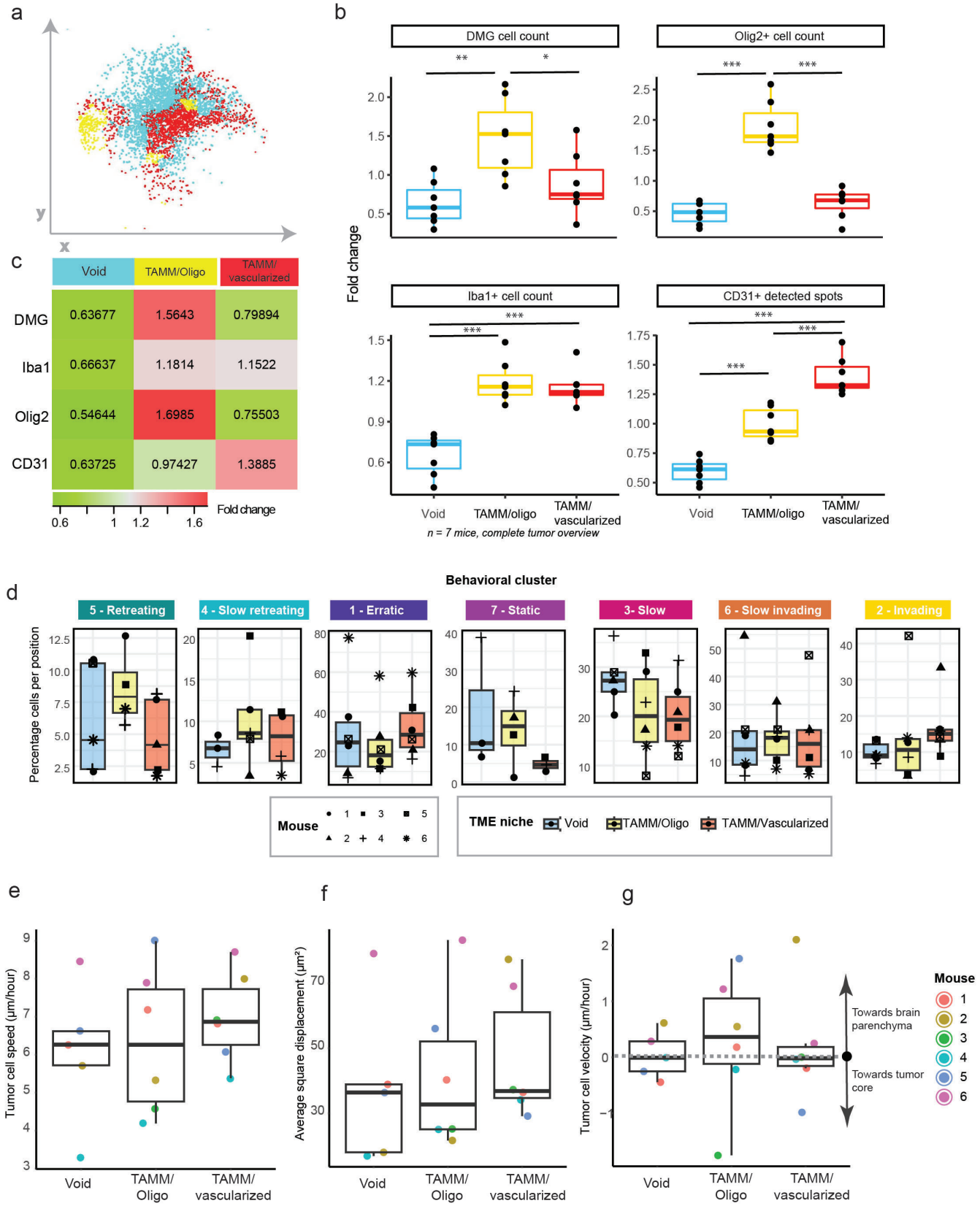

Supplementary Figure 5: Cell type and behavioral cluster frequency distribution in identified TME large-scale regions.

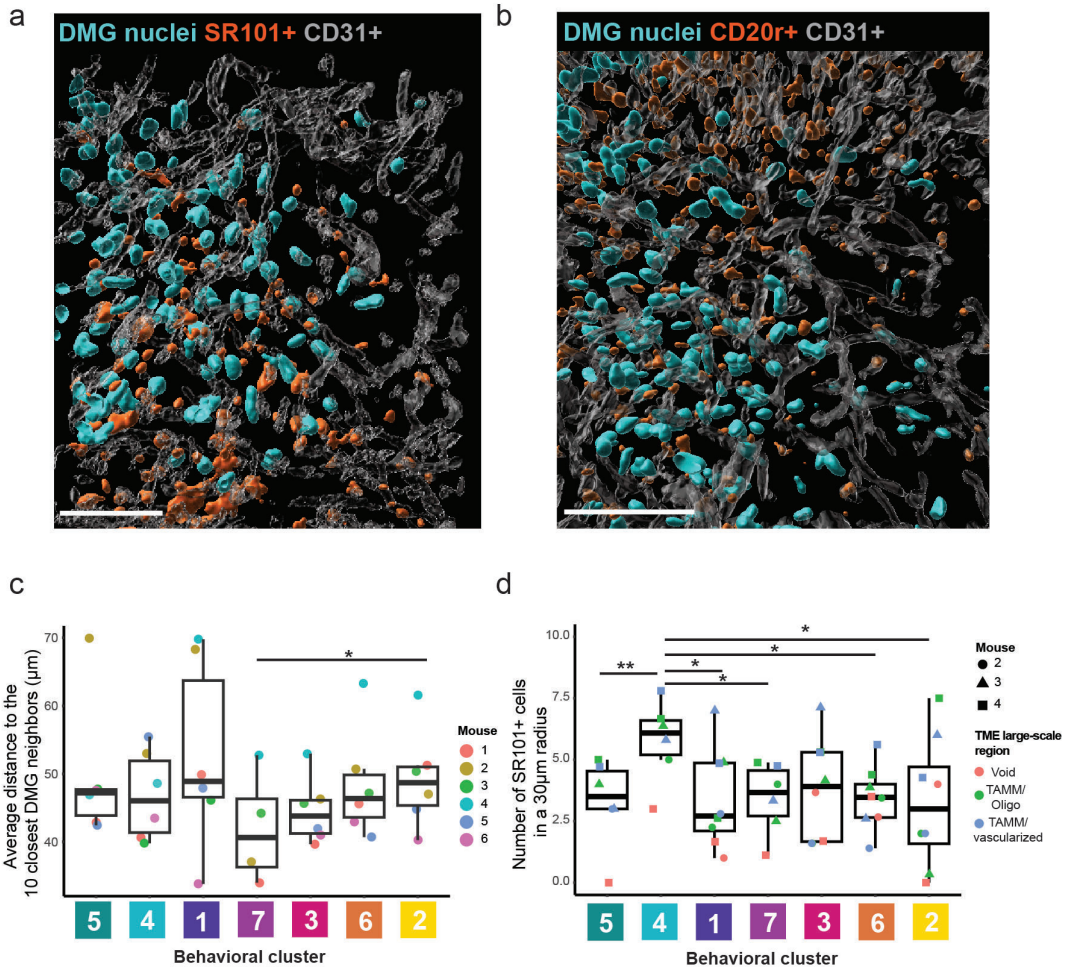

Supplementary Figure 6. Cell distribution and behavioral clusters in small-scale TME.